POLITECNICO DI TORINO

College of Civil Engineering

Master of Science program Civil Engineering

Master's degree thesis

Pavements made with HPFRCC

Thesis supervisor
Prof. Alessandro Pasquale Fantilli

Candidate
Masood Khan - s258956

Company : CEMEX

Dr. Giovanni Volpatti

Dr. Davide Zampini

March 2021

Contents

Acknowledgement

First and foremost, praises and thanks to Almighty God for His blessings throughout my life and for this thesis to be successfully completed.

I would like to express my sincere gratitude to my supervisor Prof. Fantilli for the continuous support for my thesis by dedicating his precious time to me, his availability, for his immense knowledge and motivation. This thesis would not be possible without his guidance.

Besides my supervisor, I thank my parents for their prayers, sacrifices, love and care. For their support in the decisions I made for my dreams to come true. For providing me the resources to study in a precious institute.

I would like to thank my friends who accompanied me, motivated me to keep growing through hard work and were always there for me. From them I have learned a lot.

Finally, Politecnico di Torino where I learned how challenging a student life is and accepting those challenges to come out stronger and a successful person.

Torino, 15 March 2021

Masood Khan

Abstract

Concrete has been used widely in construction of roads, highways, industrial floors and pavements since early twentieth century. Different construction methods include placement of joints after specific distances to control the transverse and longitudinal cracking due to the development of tensile stresses caused by the shrinkage of concrete and environmental factors such as temperature variation and moisture gradient. Such joints result in reduced load carrying capacity, joint failure and damage to the pavement reinforcement. As an alternative, jointless pavements can be used to reduce the joints as much as possible by adding fibers in ordinary concrete which will increase the tensile strength of the concrete, hence avoiding cracks. Stress strain models available for conventional concrete cannot be extended to UHPC or HPFRCC.

This thesis aims to describe a possible model to be used for HPFRCC as to address and mitigate possible cracking due to drying shrinkage, proper modeling and design guides are needed for the production of HPFRCC joint free slabs. A composite cross section made of concrete and soil is assumed which is subjected to an imposed strain as dry shrinkage strain and using Colonnetti's theory of elastic coactions the state of stress and strain in the concrete is calculated. Maximum tensile strain in the model is limited to the strain which produces localization and hence the cracking in the slab is avoided. This procedure is repeated for HPFRCC slab at different ages and the maximum tensile strains allowed by the concrete are compared with the maximum strains provided by the model to design the ultimate slab thickness by avoid cracking. To verify the reliability of the proposed model a possible test method is described to be used in future.

1. Introduction

Two techniques are generally used for road paving: the rigid pavement and the asphalt pavements that are cement concrete and asphalt concrete pavements respectively. Cement concrete or rigid pavement provides long term service life and excellent applicability for heavy traffic. This paving technique is easier to apply than asphalt and offers impressive cost-effectiveness and reliability. However, adequate reparation of the rigid pavement is much difficult compared to the asphalt pavement in case of deprivation or damage and requires large scale work.

Like other materials, concrete also expands and contracts with temperature variations. Concrete shrinkage starts as it cures. When the tensile stresses within the concrete overcome its tensile strength the concrete starts to crack. The tensile stresses emerge at early ages from the restriction of the volume changes of the concrete or from the temperature and moisture gradient via the concrete slab bending. The main causes of cracks in concrete pavement are hydration cracking at the early hydration state of concrete, drying shrinkage cracking caused by concrete hardening, plastic shrinkage cracking, environmental cracking triggered by thermal changes at the top of the pavement and cracking due to the long-term alkali-silica reaction process.

The drying of concrete in the first few days after placement is an important factor to the shrinkage cracking of concrete pavements. Concrete pavements typically crack in the first few days after placement as the concrete shrinks due to cooling and drying during curing and is limited by the surface on which it is placed. This restriction in the concrete slab causes tensile stresses, which increase as the slab continues to shrink over time. As the tensile strength of the concrete, which grows at a much slower rate, is reached, these stresses will break the slab. Subsequent cracks will form in the slabs over time as the concrete is fatigued from curling, warping and load-related stresses. For this purpose, by establishing a compromised plane in the slab, in order to monitor the location of the cracks, contracting joints are typically sawn in slabs at regular intervals along the length of the slab, usually within the first 24 hours. These joints can result in serviceability problems during traffic movements due to joint failure, including joint-edge chipping, uplift and

even aggressive chemicals can penetrate through these cracks and affect the long-term stability of the pavement.

Several studies have shown that there is a possibility to reduce the joints by adding different fibers (FRC, SFRC) in the ordinary concrete where the reduction of joints depend on the volume of the fibers added and the aspect ratio of fibers. In this study the use of sufficient amount of resilia HPFRCC (High Performance Fiber Reinforced Cementous Composition) to lower the crack width, lower than the maximum crack width allowed, is presented. A possible model, stage 1 model, is described in which a composite cross section made of concrete and soil is assumed and the cross section is subjected to an imposed strain ε_{sh} (shrinkage strain) and using the Colonnetti's theory of elastic coaction concrete stresses and strains are found. The maximum strain of the concrete defined by model must be lower than the allowed concrete strain and this condition must be checked at different time intervals by changing the imposed strain which varies with time and the related stress strain relationship. After finding the certain parameters which are required by the model the thickness of the slab can be found which does not need any joints in the slab or pavement.

2. Concrete pavements

The concrete pavement, also referred to as the rigid pavement, is a concrete slab made in many cases of cement, aggregate, sand, water and fibers to strengthen the characteristics of the pavement. According to different specifications, the concrete used for pavement can be changed in various ways as it needs to be solid, durable and cost-effective. Concrete pavements withstand much heavier loads than flexible pavements and are sufficient for subgrades with low strength. Concrete pavements are of various kinds:

Jointed plain/unreinforced concrete pavements (JPCP).

Jointed reinforced concrete pavements (JRCP).

Continuously reinforced concrete pavements (CRCP).

JPCP does not contain steel reinforcement but the load transfer devices called dowels at transverse joints and tie bars at longitudinal joints may be provided.

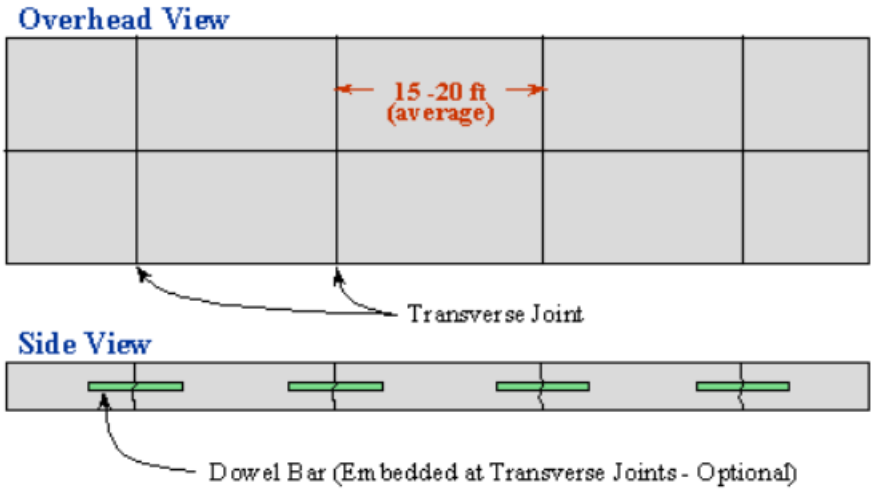

Figure 1: JPCP pavement

Jointed unreinforced concrete pavements effectiveness depends on the concrete's used tensile strength and flexural ability that can sustain cracking and the applied loads. The length of the given panel or joint interval depends on the concrete shrinkage strain produced by concrete hardening and is a process that depends on time. Unless the concrete's tensile strength is higher than the tensile stresses generated by shrinkage strain, the tensile force in the concrete generated by shrinkage strain will cause cracks in concrete.

Concrete slab thickness determines the joint intervals in the JPCP pavement. The joint spacing increases as the thickness of the slab increases, and vice versa.

JRCP is a modified version of JPCP which includes the steel reinforcement by which it is possible to reduce the slab thickness and the joint interval length can be minimized. JRCP can be designed as crack free or cracked slabs where the steel reinforcement controls the cracking in concrete and improves the stiffness of concrete slab.

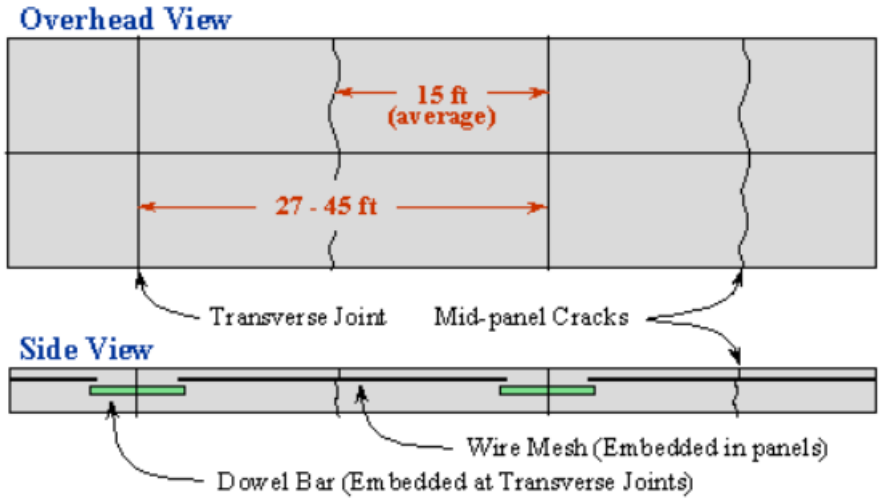

Figure 2: JRCP pavement

CRCP is a type of concrete pavement that do not need any joints for transverse contraction. The slab is supposed to have transverse fractures, usually at intervals of about (0.5 - 1.8 m). CRCP is built in the center of the slab with ample embedded reinforcement steel (approximately 0.7 percent by cross-sectional area) so that cracks can be tightly held together. Deciding a suitable distance between the cracks is part of design for this type of pavement. Due to higher amounts of steel reinforcement, CRCP typically costs more than JPCP or JRCP. They can, however, show superior long-term efficiency (typical lifetimes of design operation are 30-40 years) and cost-effectiveness. CRCP designs are used in heavy urban traffic corridors where traffic over the service life of the pavement can be in the order of tens of millions of equivalent load repetitions.

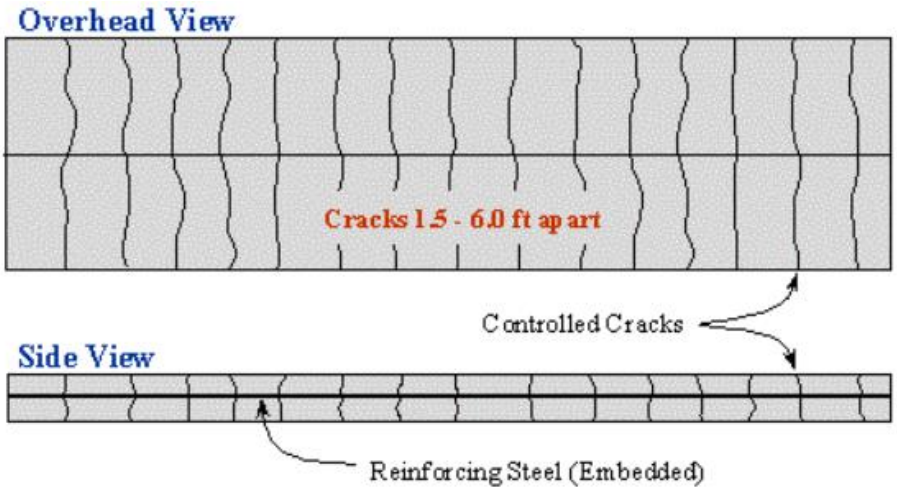

Figure 3: CRCP pavement

Concrete pavement cracking in an early age helps to relieve stress that are developed due to shrinkage, volumetric changes and restraint. Initially, the usual cracking progression occurs at intervals of 12 to 25 meters and then progresses to 5 to 6 meters. JPCP monitors the cracks by the use of joints to build a weakened plane to manage the forming cracks. CRCP's reinforcing steel provides additional restraint that allows cracks to form faster and at a shorter interval. The crack progression is quite similar, while the resulting crack spacing is shorter than the JPCP, as cracks typically form halfway between two other cracks that help to relieve tension. Most of the cracks form before the pavement is ready to traffic use, but cracking continues for the rest of the pavement life. Typically, the crack widths remain very small (usually < 0.5 mm), that helps to facilitate load transfer by aggregate interlocking.

2.1 Design of concrete pavements

The primary document used to design new and rehabilitated highway pavements is the AASHTO Guide for Design of Pavement Structures (AASHTO, 1993). All variants of the AASHTO Design Guide are empirical design methods based on field performance data assessed at the AASHO Road Test in 1958-60. The general approach of the AASHTO procedure of 1993 for both pavements (flexible and rigid pavements) is to design at the end of the pavement design life for its defined loss of serviceability. Serviceability is

defined according to the Present Serviceability Index (PSI), which differs between the ranges of 5 and 0 (best and worst). PSI, the loss of serviceability at the end of design life, is split between environmental impacts and traffic.

$$\Delta PSI = \Delta PSI_{TR} + \Delta PSI_{SW} + \Delta PSI_{FH}$$

PSI_{TR}, PSI_{SW} and PSI_{FH} are the serviceability loss components representing traffic, swelling and frost heave. In both, flexible and rigid pavements, for swelling and frost heave the structural design processes are the same; these are detailed in Appendix G of the AASHTO Guide for 1993. For flexible and rigid pavements, the structural design procedures for traffic are different. Here only the design of rigid pavements will be discussed.

2.1.1 Design equation

The empirical equation that relates pavement performance, pavement structure and traffic for rigid pavements is:

$$\log10\,(W18) = ZRSo + 7.35\log10\,(D+1) - 0.06 + \frac{log_{10}\left(\frac{\Delta PSI}{4.5-1.5}\right)}{1+\frac{1.64\times10^{7}}{(D+1)^{8.46}}} + (4.22-0.32p_t)log_{10}\left[\frac{S_cC_d(D^{0.75}-1.32)}{215.63J\left(D^{0.75}-\frac{18.42}{\left(E_c/_k\right)^{0.25}}\right)}\right]$$

in which:

W18 = Number of 18-kip equivalent single axle loads (ESALs)

ZR = Standard normal deviation

S0 = Overall standard deviation

ΔPSI = Allowable loss of serviceability at end of design life

pt = Terminal serviceability

k = Modulus of subgrade reaction (pci)

Sc = Modulus of rupture of PCC (psi)

Ec = Modulus of elasticity of PCC (psi)

J = Empirical coefficient of joint load transferred

Cd = Empirical drainage coefficient

D = Required thickness (inches) of PCC slab

Usually, the first ten parameters are the inputs to the design equation, and the output is D, the thickness. As a function of input parameters, the above equation must be solved implicitly for slab thickness D. [1]

2.1.2 Design inputs

Analysis period:

Performance period represents the time that the design of a pavement aims to last before its rehabilitation is required. Analysis period is equivalent to the time elapsed when a new or rehabilitated pavement structure starts to deteriorate from the initial serviceability to its final serviceability. Analysis period which may refer to the term performance period is the total duration that must be covered by the design policy. Realistic performance limitations, however, require scheduled rehabilitation within the required analysis period, in that case several performance periods may be covered by the analysis period. Analysis period in this context is related to the design life in the AASHTO 1993 Guide. For the analysis period of various road pavements, AASHTO recommendations are given in Table 1.

Table 1: Guidelines for length of analysis period (AASHTO, 1993)

Highway conditions	Analysis period (Years)
High volume urban	**30-50**
High volume rural	**20-50**
Low volume paved	**15-25**
Low volume aggregate surface	**10-20**

Traffic:

The most critical factors in the pavement design is the traffic, and every attempt should be made to gather the reliable data unique from every project. In traffic analysis, an assessment of the traffic growth, initial amount of traffic, directional distribution and nature of traffic is included.

A cumulative 18 kip (80 KN) equivalent single-axle load (ESALs) is the basis of the AASHTO Design Guide. However, using the below given equation ESALs can be estimated

$$ESAL = (ADT_0)\ (T)\ (T_f)\ (G)\ (D)\ (L)\ (365)\ (Y)$$

where,

ADT_0 = average daily traffic at the beginning of the design period

T = Truck percentage in the ADT

T_f = Number of 18-kip ESALs per truck

G = Factor for traffic growth

D = Distribution factor for direction

L = Distribution factor for lane

Y = Design life in years

Reliability:

Reliability of design is characterized as the likelihood of a pavement section performing satisfactorily over the design life. Uncertainties in traffic loading, environmental conditions and building materials must be accounted for. By integrating a reliability level R to provide a safety factor into the pavement design, the AASHTO design method accounts for these uncertainties and thus increases the likelihood that the pavement will work as expected over its design life. The reliability levels that AASHTO recommends for different road classes are presented in Table 2.

Table 2: Suggested levels of reliability for various functional classifications (AASHTO, 1993).

Functional classification	Recommended level of reliability	
	Urban	Rural
Interstate and other freeways	85-99.9	80-99.9
Principal arterials	80-99	75-95
Collectors	80-95	75-95
Local	50-80	50-80

In the AASHTO design equations, the reliability level is not explicitly included. Instead, it is used to evaluate the normal standard deviation Z_R. Z_R values corresponding to the chosen reliability levels are summarized in Table 3.

Table 3: Standard normal deviates for various levels of reliability

Reliability (%)	Standard normal deviation (Z_R)	Reliability (%)	Standard normal deviation (Z_R)
50	0.000	93	-1.476
60	-0.253	94	-1.555
70	-0.524	95	-1.645
75	-0.674	96	-1.751
80	-0.841	97	-1.881
85	-1.037	98	-2.054
90	-1.282	99	-2.327
91	-1.340	99.9	-3.090
92	-1.405	99.99	-3.750

Values for S_0 for a rigid pavement typically range between 0.3 and 0.45, with a commonly used design value of 0.35.

Serviceability:

The Present Serviceability Index, PSI, quantifies serviceability. Theoretically, while PSI varies from 5 to 0 but the actual range of PSI for real pavements is around 4.5 to 1.5. The initial serviceability index p_o corresponds to the road conditions immediately after construction. For rigid pavements, the standard value of p_o is 4.4. The terminal

serviceability index (*pt)* is defined as the lowest serviceability to be allowed before it becomes appropriate for recovery or reconstruction.

For the construction of major highways, a terminal serviceability index of 2.5 or higher is recommended. Therefore, a standard allowable for serviceability loss of rigid pavements due to traffic can be expressed as:

$$\Delta PSI = p_t - p_o = 4.4 - 2.5 = 1.9$$

Modulus of subgrade reaction:

The design modulus of subgrade reaction *k* is a measured quantity that is a function of the following characteristics:

- Resilient modulus of subgrade M_R
- Granular subbase thickness D_{SB}
- Granular subbase resilient modulus of E_{SB}
- Bedrock depth D_{SG} (if less than 10 feet)
- Loss of Service *LS* (erodibility index of the granular subbase)

As a primary input for rigid pavement construction, the modulus of subgrade reaction (k) is used. The layers supported below a rigid pavement surface are calculated (the PCC slab). By means of field experiments or by correlation with other tests, it is possible to determine the k-value. No direct laboratory method for the determination of the k-value exists. The reactive pressure to withstand a load is therefore in direct proportion to the deflection of the spring (which is a measure of the deflection of the slab) and k.

$$P = K\Delta$$

where,

P = Reactive pressure

K = Modulus of subgrade reaction

Δ = Deflection of slab

K value is in terms of MPa/m and ranges for weak support from around 13.5 MPa/m to over 270 MPa/m for good support. The subgrade reaction modulus is generally determined

from other stiffness measurements, but it is possible to determine in situ values using the plate bearing test.

2.1.3 Outputs

For any one of the variables, the 1993 AASHTO Guide equation can be solved if all the others are provided. Typically, the output is either total ESALs or the required slab depth (D). Usually, the rigid pavement equation mentioned above is solved simultaneously with the rigid pavement ESAL equation. The solution is an iterative method that resolves ESALs by changing the depth of the slab in both equations. The solution is iterative because there are two main factors in the slab depth (D).

The total number of ESALs that a specific pavement can accommodate is determined by the slab depth (D). From the before-mentioned design equation, it is clear that:

- For a given load, the equivalent single axle load (18KN) is determined by the slab depth.
- Therefore, designing the ESALs for the first time the slab depth D is elementary.

The deign steps according to 1993 AASHTO rigid pavement design guide are presented below as a summary:

1. Finding the analysis period.
2. Evaluation of the design traffic.
3. Determining the reliability factors for design.
4. Determining the terminal serviceability and allowable serviceability loss due to traffic.
5. Determining the effective modulus of subgrade reaction *k*.
6. Specifying the properties of PCC.
7. Determining parameters such as joint load transfer coefficient *J* and drainage coefficient C_d
8. Solving the main Eq. for the required slab thickness *D*.

2.2 Fiber Reinforced Concrete Pavements

Due to the poor tensile strength of concrete it easily gets cracked by small magnitude of external tensile forces, which leads to a corrosion of the steel reinforcements, a loss of its durability and a reduction in its service life. Crack generation in concrete can be prevented by increasing its tensile strength or adding multiple discontinuous fibers. In order to produce cracks in concrete having a higher tensile strength, a higher tensile force must be applied, thereby limiting the frequency of cracks. Also, the presence of discontinuous fibers can effectively prevent the formation, propagation and widening of micro-cracks. They can also marginally increase the tensile strength and significantly control the widening of cracks. [2]

Fiber reinforced concrete FRC pavements are more effective than ordinary cement concrete pavement in crack propagation. FRC is described as a composite material consisting of concrete reinforced with discrete short-length fibers that are randomly but uniformly distributed.

Usually, fibers that are used in concrete pavements are made of steel or synthetic fibers and come in a range of lengths, forms, sizes, and thicknesses. During the process of batching and blending, they are added to fresh concrete. The main differences between fibers and conventional steel reinforcement are location, length and area of cross section of fibers. Instead of being mounted at particular pavement positions, fibers are uniformly dispersed across the concrete, fibers are much shorter than continuous steel reinforcements, and take up a much smaller pavement cross-sectional area than conventional steel reinforcement.

2.2.1 Synthetic Fibers

Materials such as aramid, acrylic, nylon, carbon, polyester, polyethylene or polypropylene are made from synthetic fibers. The use of synthetic fibers in concrete has been in practice for a past few decades To date, their main application in concrete pavements is the use of ultra-thin white topping, where 5 to 10 cm of concrete is bonded to have a composite pavement with an existing asphalt pavement.

Fibrillated polypropylene made synthetic fibers are most widely used fibers in the concrete pavements. Fibers are usually added at a rate of at least 0.1 percent by volume in concrete. Ultra-thin white topping commonly utilizes polypropylene (or polyolefin) fibers of 1.8 kg/m^3. Decrease in plastic shrinkage and cracking, improved resilience or post-crack integrity, are the advantages of polypropylene fibers.

Polypropylene fibers in fresh concrete often eliminate the aggregate particle settlement from the pavement surface, that results in a pavement which is skid resistant, less permeable and more durable.

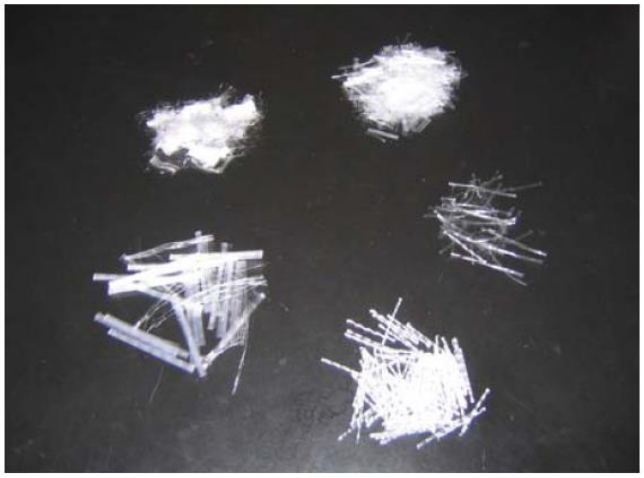

Synthetic fibers come in a variety of shapes, sizes, and properties.

Figure 4: Synthetic fibers

2.2.2 Basalt fibers

Basalt fibers due to their characteristics, which include good mechanical characteristics, especially high strength, high elastic modulus, high thermal and chemical stability and good sound insulation properties they have been investigated by few researchers during the last decade. Higher energy absorption ability after attaining the optimum load and improved ductility are the prominent characteristics endorsed by Basalt fiber reinforced concrete. In addition, it is also noted that, unlike other fibers that cause difficulty in handling and therefore form balls such as steel and polyvinyl alcohol PVA fibers, basalt fibers are easy to disperse in the concrete mix without segregation and lose of shape due

to their flexibility. Similar results are also reported in other studies that have shown encouraging effects of basalt fibers on concrete strength and resistance to cracking.

In a study conducted by Tehmina et al. [3], higher basalt fiber fiber volumes varying from 1 to 3 percent in three different HPC mixes are used to assess the compressive strength, elasticity modulus and splitting tensile strength. The results of maximum cylindrical compressive strength showed the small increase in the compressive strength up to 2% fiber volume; however, at 3% fiber volume, compressive strength was observed with a decrease in value from 2.37% to 15.1%. Similarly results of splitting tensile strength showed that the use of basalt fibers in volume of 1, 2 and 3% enhances the tensile properties of concrete.

Figure 5: Basalt fibers

2.2.3 Steel Fibers

Steel fibers are being used in road construction and in flooring for a long time, particularly where there is heavy wear and tear. Through the transfer of forces between fibers and matrix, the bond behavior in SFRC is achieved through interfacial bond. Physical and chemical adhesion, mechanical anchorage, friction, fiber to fiber interlock are the main bond components. According to SFRC studies, the tensile behavior shows that it increases the strength of the tensile concrete, improves the post-peak tensile concrete behavior, which depends on the efficient fiber crossing the crack. Steel fibers are generally between

12.7- 63.5 mm and 0.45-1.0 mm in length and diameter respectively. The typical volume of steel fibers ranges in concrete mix is from 0.25% to 2% or 20-157 kg/m^3.

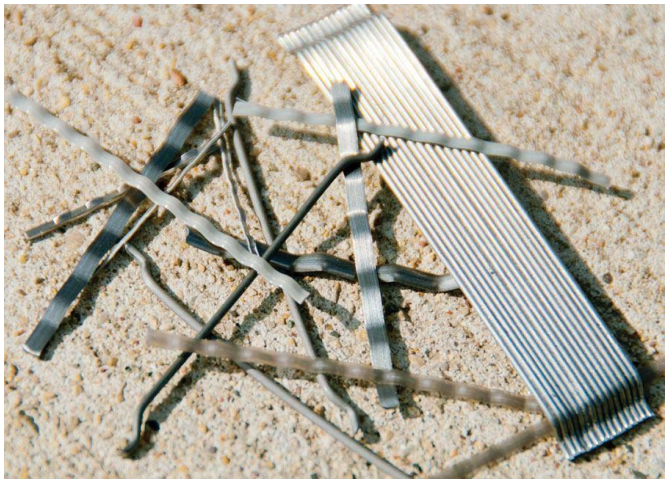

Figure 6: Steel fibers

Shrinkage cracks lead to an increase in maintenance cost and reduced serviceability because of reduction in concrete load-carrying capacity and they accelerate deterioration. Two common types of shrinkage are plastic shrinkage and drying shrinkage. High rate of water evaporation at an early age of concrete results in plastic shrinkage cracks, some other factors like autogenous deformation and differential settlement also effect plastic shrinkage. Contraction of the hardened concrete due to the excessive capillary water loss is known as drying shrinkage.

Steel fibers in concrete are used to delay and control the tensile cracking in the composite material. This positively impacts concrete's mechanical properties. These enhanced properties have made SFRC a viable material for concrete road pavements.

The studies show that the use of various fibers to strengthen concrete properties against shrinkage cracking is very effective in protecting pavements and depends on the volume of the fibers and their aspect ratio for their effectiveness. Out of other studies done by using different fibers, a study was done by *Y. CHOI et al*. [3] using macro fibers of three different kinds with their lengths longer than 30 mm and small aspect ratio along with micro nylon fibers with their lengths of 12 mm and the aspect ratio larger than 1000 tests were caried out. Tests were performed using micro and macro fibers with either a single

type of fiber or hybrid fibers, and the fiber volume ratio used was 0.2 to 0.3% of the concrete pavement mix. Using the so-fabricated specimens, strain caused by drying shrinkage and autogenous shrinkage of concrete was analyzed comparatively. The results demonstrated that by using the of 0.2% volume of nylon fibers, the drying shrinkage strain can be significantly reduced to about ¼ compared to the non-reinforced plain concrete and that the hybrid fiber reinforcement mix resulted in remarkable reduction of the autogenous shrinkage.

3. Jointless pavements

Jointless or CRCP is a kind of PCC pavement having steel reinforcement through its entire length. It is a kind of concrete pavement which does not require any transversal contraction joints. Random cracks are generated in the entire pavement by using the continuous reinforcement thus eliminating the requirement of transversal contraction joints which are vulnerable to joint-related distresses and failures. The use of reinforcement holds the cracks securely without the concern if the cracks are evenly spaced, which preserves the structural integrity of the pavement. For this type of pavement, deciding a suitable distance among the cracks is a design process part. Owing to higher amounts of steel reinforcement, jointless pavements typically cost more than other types of pavements. They can, however, offer cost-effectiveness as well as superior long-standing efficiency.

Through its exclusive nature, ensuring the long life of pavement and low maintenance expense, and providing excellent foundation for future overlays, the high durability and strength characteristics of jointless pavements are obtained. In addition, high riding efficiency can be provided by removing transverse contraction joints. They need to be planned and properly installed in order to have a benefit or otherwise the pavement will fail prematurely due to continuous increase in heavy loads from traffic. Reinforcement ratio, thickness of pavement, material properties of concrete which are determined by the type of coarse aggregate, w/c ratio, quality of subbase and drainage, and placement of steel rebars are the design and construction features that significantly affect CRCP's performance.

The procedure for designing the pavement thickness in case of CRCP is similar to the design of thickness in case of jointed pavement in the AASHTO design guide except the only difference between both of the methods is the load transfer coefficient which is slightly smaller in CRCP compared to jointed pavement which results in smaller slab thickness in case of CRCP.

Nomographs which are developed from the empirical equations are used for longitudinal reinforcement design while using AASHTO design. Tensile strength of concrete, shrinkage, diameter of steel rebar, design temperature, tensile stresses due to wheel load

are the input data for designing jointless pavements. Three limiting criteria needs to be considered while designing jointless pavements: crack width, crack spacing, and stresses in reinforcements. To insure the acceptable performance of jointless pavements under predicted traffic loads and environment the acceptable limits of three criteria is mentioned below. [4]

- Crack spacing: Considering punchout failure and spalling, the crack spacing is limited to a specific value. Maximum spacing between cracks in order to avoid the spalling is limited to 2.438m and maximum crack spacing to avoid the punchout failure is limited to 1.067m.
- Crack width: This limit is based on considering the water penetration into the pavement and spalling. The maximum crack width allowed should be less than 1mm. By the use of higher percentage of reinforcement or rebars of small diameter the crack width can be minimized.
- Reinforcement stress: This criterion is set to limit the excessive permanent deformation of steel rebar and fracture. 75 percent of ultimate tensile strength of rebar is recommended to avoid this stress.

The adopted steel reinforcement ratio varies around the world. 0.6 percent is the most widely used quantity of reinforcement. 0.7 percent of the volume of steel is favored in more extreme weather conditions.

3.1 With UHPC

As compared to asphalt, the concrete hardening time has long been regarded as a weakness. Although asphalt pavement can be trafficked as soon as the temperature of the asphalt has dropped down to a value similar to the ambient one it is necessary to wait several days or several weeks before to ride a concrete pavement. However, a high early strength or ultimate high early strength (HPC/UHPC) can be used by saving the time and resources so the use of UHPC in pavement can lead to quick works with a minimal traffic interruption.

High performance concrete and ultra-high-performance concrete are currently being used for the pavement constructions either jointless or where there is a need for rapid repair and the early use of the pavement is necessary. Use of fibers to increase the compressive strength, tensile strength, crack resistance against shrinkage of concrete has been considered one of the most efficient method. These kinds of pavements are made mostly with steel fibers and their performance is quite satisfactory for a long period of time. Besides steel fibers other fibers like glass, basalt is also used for increasing the compressive strength, tensile strength and improving shrinkage resistance for controlling crack width. Several studies done on high-performance concrete and ultra-high-performance concrete shows that their strength highly depend on the matrix strength, which is from normal to high strength, bond strength between fibers and matrix, fiber characteristics like volume of the fiber in the matrix, shape and size.

3.1.1 Matrix and fiber properties effect on UHPC strength

Parameters effecting the mechanical response of UHPC have been discovered by many researchers. Dosage of fine mineral admixtures, size of aggregates, effect of the size of specimen, curing condition are the factors which highly influence matrix properties. Water to cement ratio is also an important factor which controls the concrete slump and its high strength especially in the presence of fibers, steel fibers, in UHPC. According to the research the tensile properties of UHPFRCC are also affected by the fiber properties.

Effect of matrix strength and fiber type of different steel fibers on their pull out behavior in UHPFRCC was studied by *Yoo et al*. [5]. Results showed that maximum stress in the fibers and their bond strength increased with the increase of matrix strength for all the fibers. At the initial normalized slip hooked steel fibers showed a greater fiber stress compared to the straight fibers, irrespective of matrix strength, but after the normalized slip the fiber stress provided by straight fibers was comparatively more. This proved that in case of large crack widths straight fibers are much better than the hooked fibers. For average bond strength the use of short fibers, straight, for an increased matrix strength is better than long fibers. With an increase in fiber length and decrease in its diameter the maximum fiber stress also increases. For the tensile strength of concrete, the most

important property is its fiber properties rather than matrix strength because fibers will bridge the cracks.

Response of hooked versus twisted fibers on the pull out response on different matrix strengths of 28MPa, 56MPa, 84 MPa concrete was studied by *Kim et al*. [6]. They concluded that by increasing the matrix strength, and the twisted fibers as compared to hooked fibers are more subtle to the matrix strength for higher pullout resistance. *Chao et al.* [7] studied hooked fibers and twisted polygonal steel fibers where twisted polygonal steel fibers showed a high level of resistance against slips. Results from direct tension tests showed that the specimen with twisted steel fibers of 2 percent volume exhibits a tensile-hardening behavior with a peak strength of 11.7 MPa and tensile strain of 0.6 percent, which led to multiple crack formation in comparison to the 2 percent volume of hooked fibers with a strain of only 0.2 percent. The longer fiber offers due to their longer embedded lengths provides better resistance against cracks by bridging effect compared to short fiber where effective bridging against cracks can be obtained by increasing their fiber volume.

Another parameter for increasing mechanical properties of concrete is the water cement ratio. As the water cement ratio decreases, even though these properties do not expand as fast as the compressive strength, the tensile strength can be easily doubled when moving from regular to high-strength concrete. The thickness of concrete slabs can therefore be decreased, but the reduction is limited by the increase in E-modulus, which for a given deflection produces a higher tensile stress. Although concrete slabs are typically constructed based on fatigue calculations, the conditions of interaction with the base course play a crucial role in the long-standing occurrence of cracking. The concrete shrinkage, which causes the curling phenomenon, governs these contact conditions. The drying shrinkage is usually decreased compared to ordinary concrete with a UHPC. A decrease in drying-induced curvature is beneficial for a longer pavement life, everything being equal.

Regarding material durability, it is well known fact that when the water cement ratio of the material is decreased, most of the concrete properties develop in a positive direction. The carbonation depth, for example, becomes negligible, the electrical resistivity increases, and the permeability of the chloride decreases. Of course, this is advantageous

with respect to the possibility of steel corrosion in continuously reinforced concrete pavement or jointless pavement. The resistance to freezing and thawing is also improved, to the point that air can become superfluous. UHPC, in principle, is highly appropriate for the construction of durable and thin roads. However, the practical implementation on the site reveals several difficulties. The preparation of such high-tech concretes needs more constituents than ordinary mixes in the production state, such as superplasticizer, silica fume or fibers, the local aggregate must be replaced by a better-quality aggregate, and UHPC systematically requires longer mixing time than ordinary concretes.

Different developments in different parts of the world were carried out using UHPC for constructing thin concrete pavements as well as for instant repairs or quick renewal of roads. Burger et al**.** [8] used UHPC containing cement, fly ash, silica fume, polypropylene and steel fibers with a 28 day compressive strength of 90 to 120 MPa and a flexural strength higher than 10 MPa. *Hachiya et al*. [9] investigated the use of HPC in airport pavement with a view of reducing slab thickness. The cement content was increased from 340 kg/m^3 to 450 kg/m^3, the water to cement ratio went down from 0.4 to 0.3; the design flexural strength increased from 5MPa to 6.5 MPa which allowed a reduction of slab thickness from 420 mm to340 mm. Similarly, *Alte-Teigeler* [10] used UHPC for a quick renewal of damaged highway slabs where the special mixture developed very early strength with values of 20, 50, 80 MPa at 4 hours, 24 hours and 28 days respectively. The total renewal operation took 5 to 7 hours and after that more than 1000 slabs had been treated in Germany with his technology.

3.2 Mechanical properties of HPC/UHPC

3.2.1 Compressive strength

Compressive strength, which is the most important property in the design of any reinforced concrete structure, of UHPC varies 150 to 250 MPa. Until 70 percent to 80 percent of the compressive strength of UHPC it is a linear elastic behavior.

The linear behavior of UHPC is shown in Figure 7, stress-strain-diagram, and it shows that without the presence of fibers there will be a sudden rupture and the failure is explosive in nature. Compressive strength can be improved by introducing fibers in

UHPC. Figure 8 shows a typical stress strain curve in case of fibered UHPC where because of cracking and bridging fiber effects there exists a descending branch of the curve. Descending parts range depend on the volume of the fibers as well as their shape.

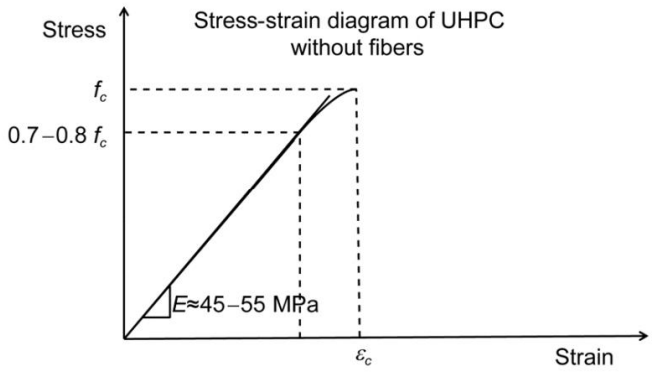

Figure 7:Compressive stress-strain-diagram of UHPC without fibers

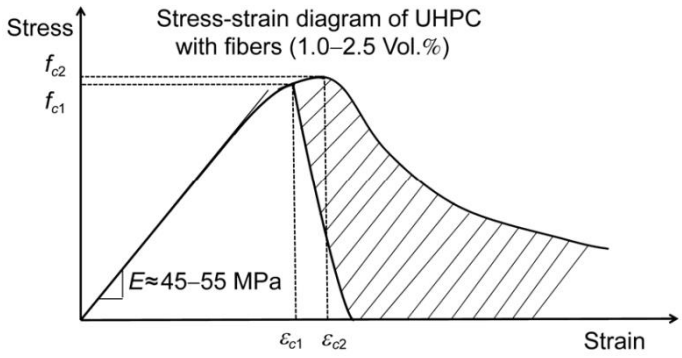

Figure 8:Compressive stress-strain-diagram of UHPC with fibers

3.2.2 Tensile strength

Tensile strength of UHPC varies normally from of 7 to 15 MPa depending on fibers volume and type and their tensile behavior becomes ductile due to their bridging effect of fibers.

Figure 9 shows the tensile stress strain response in case of UHPC proposed by *Graybeal* [11] which is based on direct tension tests on two UHPC specimen with multiple fiber contents. The tensile behavior can be divided into four different phases. Elastic phase,

Phase I, when the matrix stands the loads. The multi-cracking phase, Phase II, in which a number of tightly spaced multiple cracks in UHPC matrix are formed where cracks are produced when the stresses in the matrix exceeds its tensile strength. The strain hardening phase, Phase III, in this phase the individual cracks in the matrix become wider but no new cracks are formed. Finally, the strain softening phase, Phase IV, where cracks start to localize, and fibers start to being pulled out from the matrix after which the material fails. Tensile stress-strain curve might not be as exactly as illustrated in Figure 9 because of the fact that the post cracking behavior of UHPC (phases II, III and IV) is largely dependent on the volume, type and orientation of the fibers in the matrix. If the fiber volume is too low or not at all, there will not be phases II, III and IV.

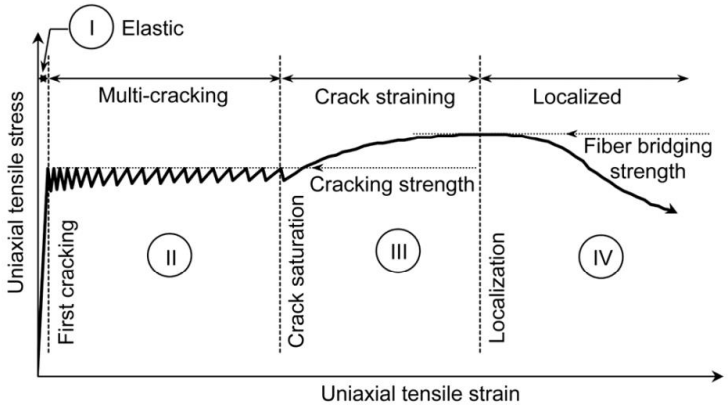

Figure 9: Idealized uniaxial tensile response of UHPC

3.2.3 Shrinkage in UHPC

In UHPC, as the shrinkage develops at early age, its effects are superimposed to those of thermal shrinkage. Plastic shrinkage and drying shrinkage are two main sources. The cracking due to plastic shrinkage is primarily because of water evaporation rate, which is higher at an early age, while other driving forces are also influential, such as differential settling, and autogenous deformation. Contraction of the hardened concrete due to the excessive capillary water loss is known as drying shrinkage.

Due to low w/c ratio and water loss, tensile stress builds up in the presence of constraints, resulting in cracking until the tensile strength of concrete is reached. Although normal strength concrete bleeds do not exhibit any bleeding but after casting UHPC, a large

cracking pattern occurs which is very difficult to fix if successful curing is not applied within a few tenths of minutes. Furthermore, ground settlement or swelling also alters a slab's boundary conditions and contributes to cracking. The drying shrinkage rate may also be negatively affected by construction-related problems such as concrete transportation, installation of slab, and finishing of the slab. Long duration hauls in a concrete transit mixer, excessive temperature of concrete, addition of water in concrete mix on site, and failure in the protection of slab from wind affect shrinkage of concrete in the initial stages. For a joint-free floor to be successful, it needs the minimum contraction and minimum restraint along its edges.

Drying shrinkage development in both cases, UHPC and HPC, is same. Drying shrinkage in case of UHPC is lower than that of HPC because of the lower water cement ratio, the presence of fibers, and higher density of the matrix. Drying shrinkage can be negligible at the end of heat treatment of UHPC.

A research on total shrinkage mitigation for ultra-high-performance concrete was conducted by *Valipour et al***.** [12] which evaluates the efficiency of different approaches for mitigating drying shrinkage as well as autogenous shrinkage for UHPC. Study included MgO-based and CaO-based expansive agents in various contents, pre-saturated lightweight sand, and shrinkage-reducing admixture. UHPC mixtures were subjected to moist curing for the periods of 1, 3, and 7 days and their compressive strength development, autogenous and dry shrinkage were evaluated. Test results showed that by using lightweight is more effective in reducing shrinkage than increasing its compressive strength. Replacing by volume, the natural sand by 60 percent of lightweight sand, it was found the reduction in autogenous shrinkage from 530 to 35 mm/m at 91 day. With the use of 60 percent lightweight sand in volume either with MgO based or CaO based expansive agent or with shrinkage reducing admixture the 91day dry shrinkage is reduced by 700mm/m while autogenous shrinkage by 600mm/m. On mitigation of total shrinkage, the initial curing period is of highly importance.

3.3 Strength prediction models

The HPFRC's mechanical behavior is influenced by the reinforcing fibers' engineering properties, the concrete matrix, and interaction between them. It is significant to understand how the compressive strength and tensile strength of an HPFRC differ when the ratio l/d_e, volume of fibers V_f and shape of the fibers are altered for practical purposes. These models, based on a particular matrix, allow us to understand which type of fiber and what quantity of fiber is necessary to fulfill the requirements of the designers.

With respect to normal concrete, HPFRCC have much higher mechanical properties due to which the strength prediction models of normal strength concrete are not applicable to them. Predictive models are useful in order to reduce the number of tests required to completely understand what is the minimal quantity of fibers which is required for a certain tensile strength to be achieved.

In Literature, multiple predictive models were found. A linear model was developed by *Ramadoss et al*. [13] to predict the compressive strengths and splitting tensile strengths of three mortars by increasing V_f from 0 to 1.5 percent of a single type of steel fiber. Thus, this model is applicable if the fiber's *l/de* ratio is not changed:

$$f_{cf} = f_c + 0.0184 * RI \qquad (1)$$

$$f_{spf} = f_{sp,matrix} + 0.006 * RI \qquad (2)$$

where, $RI = w_f * l/d_e$ and $w_f = \left({}^{fiber}/_{density}\right) * V_f$

Savino et al. [14] predicted model using V_f and fiber's *l/de.* The model is predicted for V_f ranging from 1.5 to 5%. In the equations below, R^2 is coefficient of correlation.

$$f_c = 75.1436 + 0.0499 * {}^{l}/_{d_e} + 4.4016 * V_f(\%)\,; \qquad \text{with } R^2\text{=0.84} \qquad (3)$$

$$f_t = 3.5119 - 0.0178 * {}^{l}/_{d_e} + 1.876 * V_f(\%)\,; \qquad \textit{with } R^2\textit{=0.78} \qquad (4)$$

Savino et al. [15] studied four types of steel fiber shapes, aspect ratios and four fiber volumes. The relationship between experimental data and the model confirmed not only the prediction of mechanical properties of UHPFRCC but it also tells the suitable combination of fiber properties and the matrix strength so that the minimal fiber dosage can be selected for required strength beforehand hence reducing the manufacturing cost. For post-cracking behavior, fiber orientation also affects strongly the peak strength and its energy-absorbing capability. The study took into account straight steel fibers and hooked end steel fibers and they both showed different behaviors, hooked-end fibers with increased strength than straight fibers, so two models are presented based on the shape.

$$f_{c,sf} = 1.067 f_{c,matrix} + 5.9652 l - 393.2199 d_e + 3.3258 V_f \;; \qquad R^2 = 0.92 \qquad (5)$$

$$f_{t,sf} = 0.9788 f_{t,matrix} - 0.9309 l + 59.6367 d_e + 1.2677 V_f \;; \qquad R^2 = 0.91 \qquad (6)$$

$$f_{c,hf} = 1.3757 f_{c,matrix} - 0.8456 l - 17.7099 d_e + 7.0429 V_f \;; \qquad R^2 = 0.90 \qquad (7)$$

$$f_{t,hf} = 0.8526 f_{t,matrix} - 0.0747 l - 5.3867 d_e + 08551 V_f \;; \qquad R^2 = 0.90 \qquad (8)$$

where,

$f_{c,sf}$ and $f_{t,sf}$ are compressive and tensile strengths of straight fibers, $f_{c,hf}$ and $f_{t,hf}$ are compressive and tensile strengths of hooked-end fibers.

V_f and *l/de* are fiber volume and aspect ratio, R^2 is the coefficient of correlation.

4. Possible Model

The use of different kinds of fibers in design and construction of jointless slabs has already been discussed where the design includes the controlled crack patterns in the slabs in order to avoid joints. The area of such jointless slabs is governed by the concrete shrinkage tensions, as they will go beyond the tensile strength of the concrete the cracks will start to appear. This shrinkage usually starts at the early age of concrete when it is starts setting and curing and is affected by the external factors such as transportation and laying of the concrete, the finishing of the slab, loss of excessive capillary water. Using of FRC for increasing the tensile strength of concrete and to control the shrinkage crack width to be lower than the minimum crack width defined by the code is already in practice.

Destrée et al. [16] discussed the main factors affecting drying and shrinkage which are categorized into these three points:

1. Matrix properties of concrete.
2. Fibers internal restraint effect.
3. Effect of base friction on external restraint.

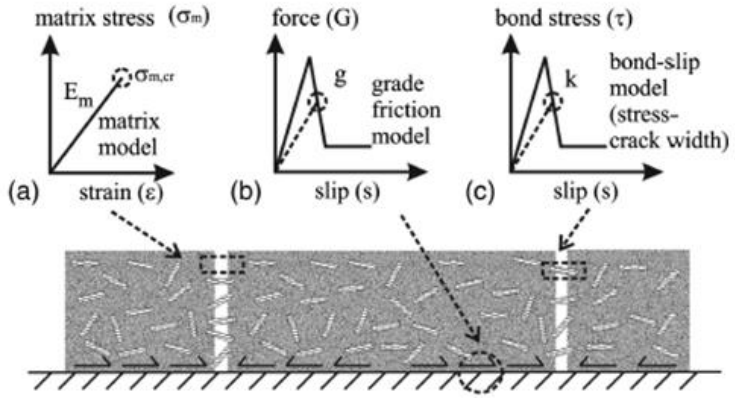

Figure 10: Mechanical behavior and finite-difference model of cracked fiber-reinforced cement composite: (a) matrix strength for cracking criterion; (b) nonlinear spring model simulating the frictional force; (c) bond-slip model

Use of excessive water in concrete will increase its porosity and will result in moisture loss hence shrinkage, water reducing admixtures, low aggregate content. Aspect ratio of the fibers, shape, and their volume will affect the relationship between stress crack width

and fiber matrix bond as they are responsible for creating a bridge between microcracks and restrain their growth from turning into macrocracks. With various frictional restraint levels, there exists a significant variation of base frictional restraint. Weight of slab and its coefficient of friction controls the interlocking properties so as the base rigidity increases against sliding friction the restraint increases as well. Field experiments have shown that with the base of higher stiffness value the crack widths are smaller for a joint free slab.

A model for FRC is provided by Destrée et al. [16] which is based on classical tension stiffening phenomenon of RC structures:

- The response of soil is as of the steel.
- There is a bond slip mechanism amid concrete and soil.
- Fracture mechanics is used to model the cracked FRC in tension.

The parametric study indicated that the with higher levels of restriction, the expected crack opening was reduced by increasing fraction of fiber length, support friction, and the bond strength. It shows that both, fiber and base course, plays an important role in controlling the crack openings by limiting the movement of segments of a cracked slab.

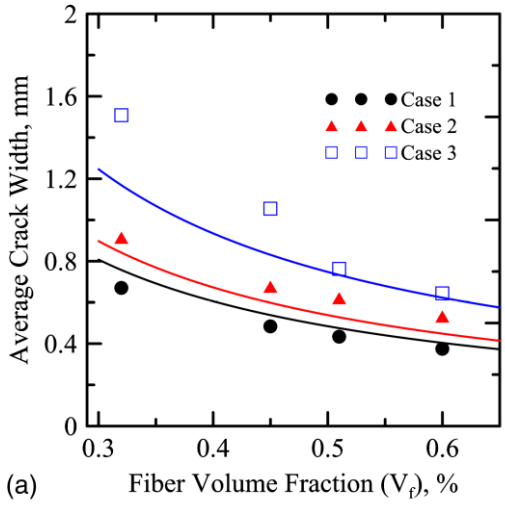

Figure 11: Effects of steel fiber content

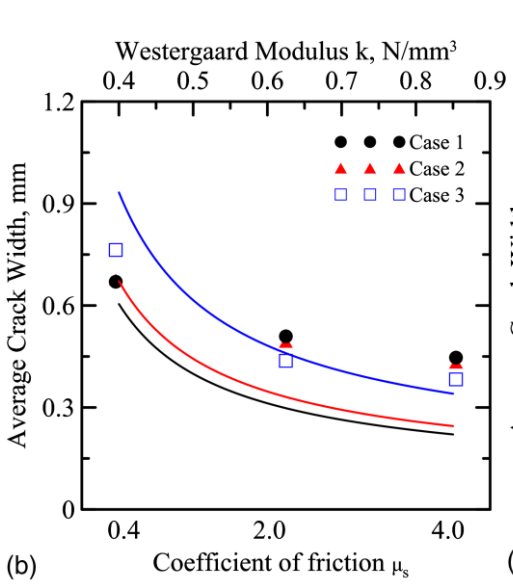

Figure 12: Effect of coefficient of friction μs

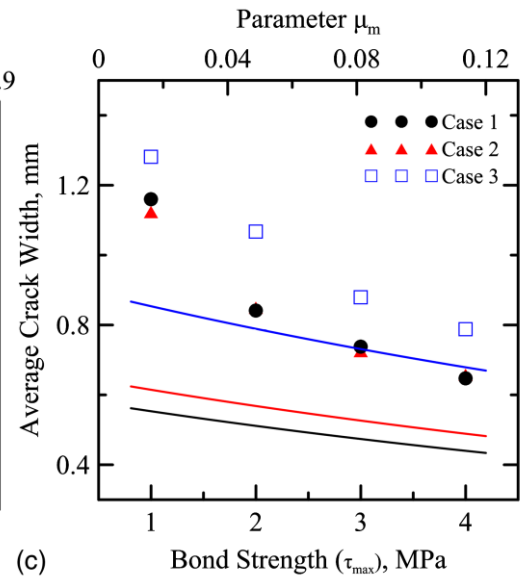

Figure 13: Effect of bond strength

As shown in Figures 11,12,13 there is a linear relationship between the stress and the strain up till the cracking then after that there is a residual stress because of the bridging effect of fibers and crack width will be controlled with this residual strength which of course depends on the volume of fibers used. The result of changing fiber volume can also be seen on the crack width, as the volume increases for any of the three cases the crack width reduces. So, doubling the fiber volume will reduce half the crack width.

Although the model predicted for FRC is an improvement in the jointless slabs using steel fibers, but it cannot be applied on the UHPC and HPFRCC because in them the strain localization in tension does not occur at cracking. Also, the evaluation of crack width with time is not discussed. Hence, with or without fibers, concrete can't produce the tensile strains which are fully compatible with the strains of steel rebars so there is a bond slip and the development of crack is because of the bond-slip mechanism between concrete and steel.

As shown in Figure 14, in HPFRCC the strain at maximum stress is larger than the steel strain at yielding so the strain incompatibility vanishes.

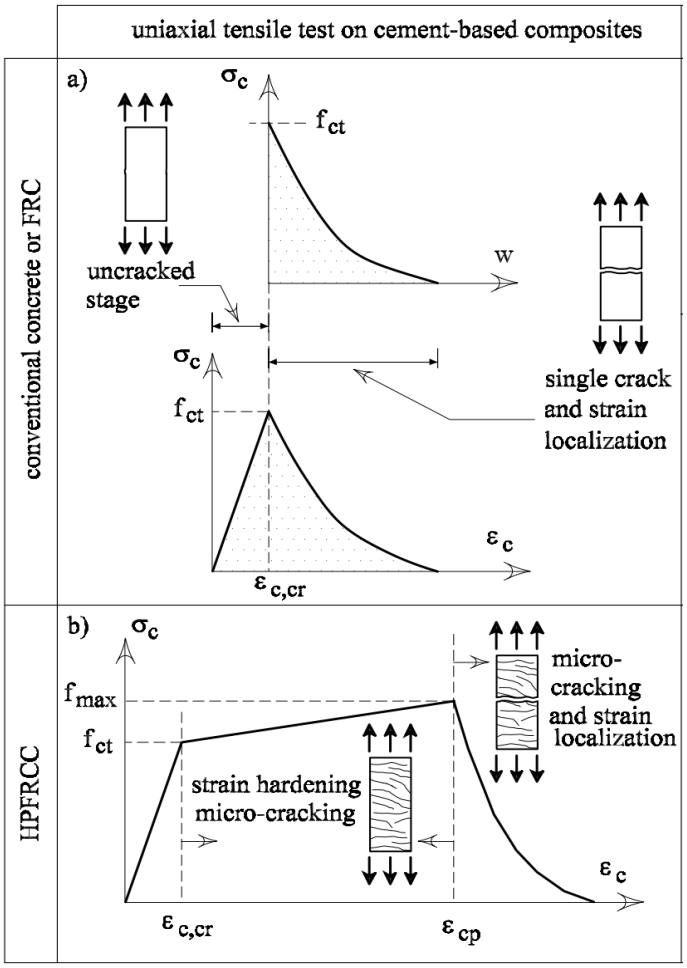

Figure 14: Uniaxial tensile tests on Cementous composites and their response

To overcome this problem a new FRC called HPFRCC is considered.

4.1 Using HPFRCC

HPFRCC, high performance fiber reinforced cementitious composite is a cluster of fiber reinforced cementous based composites which has a exclusive ability to exhibit strain hardening behavior accompanied by multiple cracking under tensile loading. They have the ability to plastically yield and harden under high loading and are more resistant to cracking so they last longer than FRC.

Binder content of HPFRCC is higher compared to an ordinary FRCC, HPFRCC contains at least one of these materials, silica fume and granulated blast furnace slag, fly ash, and steel fibers. Fundamental role of HPFRCC is to provide an increased mechanical

properties and durability. They are described as ceramic like materials having low porosity because of their low shrinkage properties, high durability, dense microstructure, and higher strength.

HPFRCC developed by different researchers demonstrated that they have ability to generate several evenly distributed microcracks avoiding macro cracks which result in serious problems. In addition, they exhibit strain hardening behavior and can withstand higher deformations with respect to traditional fiber reinforced concrete. Once the strain hardening starts, HPFRCC creates finely distributed cracks until the member fails after the strain localization. As the tensile properties of HPFRCC are much different from FRC, different researchers investigated their tensile behavior and predicted relationships between stresses and crack widths.

Removing coarse aggregates and optimizing the granular mix, incorporating pozzolanic materials and application of heat at 90 °C are the elementary principles of developing UHPC. Addition of some steel fibers is beneficial for improving UHPC tensile strength and ductility. These concepts make it possible to acquire a homogeneous and highly dense cement matrix which provides ultra high compressive strength between 170 MPa to 230 MPa and flexural strength between 30 MPa to 60 MPa, and ultimate tensile strain at peak stress up to 1.1 percent and tensile strength up to 10 MPa [17]. With such high mechanical properties, HPFRCC is an innovative material and a solution to the problems which conventional concretes do not provide.

As we know that joints are provided because of shrinkage, when the concrete is placed on the ground it shrinks so there is a friction between slab and the soil which creates an internal strain and the internal state of stress which creates cracking. By using the HPFRCC the joints can be placed at exceptionally greater distances and even there is a possibility to remove the joints at all, the jointless slabs. So, the goal of this study using HPFRCC is to eliminate joints completely. So, this interaction is similar as a cross section between steel and concrete, steel has a same function as that of soil and vice versa. Concrete tends to reduce its volume and steel contrasts its reduction in volume and in case of slabs on ground the soil contrasts against the reduction of concrete volume.

The common amount of fibers added in the normal concrete is around 0.6% but if we add larger amounts like 1 to 2% in volume than in this case, we will have a new behavior. In

this behavior, represented in Figure 15, when we have a crack there will be no softening at f_{ct} but hardening up to a new value f_u. The difference between two cases is that in the case of lower fiber volume, when there will be a single crack at the value f_{ct} and after f_{ct} there will be strain localization and the section will be called as Stage II cross section. But with the case of greater fiber volume there will be a first crack at f_{ct} then there will be multiple cracks at f_u. After f_u there will also be a softening because of the strain localization, this cross section will be called as Stage I cross section. The evolution of crack pattern is generally because of the bond-slip mechanism among concrete and steel, which allows the transfer of tensile stresses in the concrete also.

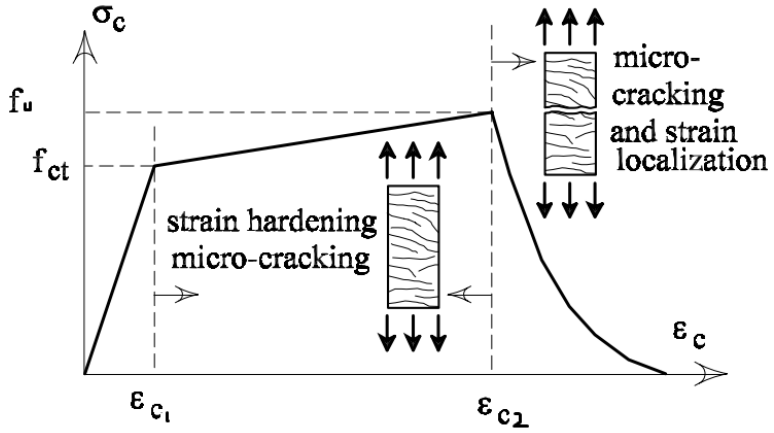

Figure 15: Stress strain relationship with HPFRCC

In Stage I cross section there exists a perfect bond between concrete and steel and the crack width is practically zero means concrete and steel with maximum stress. In Stage II the cross section acts in a different way where after cracking only concrete is in compression and steel in tension, so the part of the concrete in tension is reduced and there is no more a complete cross section contributing to the strength. In Stage I the strain $\varepsilon_{c1} \leq \varepsilon_{c2}$ and concrete is in tension and contributes to the whole cross section, in practice this type of concrete behaves similar to steel where we have plastic behavior.

When the strain incompatibility vanishes, the mechanical response which is the load versus average steel strain (N vs ε_m) can be calculated by the Stage I model instead of solving the tension stiffening problems. Figure 16, represents the stage I model curve where there is no slip between concrete and steel and concretes post peak behavior is considered

to be perfectly plastic. In this situation there are no wide cracks because of the strain compatibility between materials, zero localized deformations in concrete. When a RC element is subjected to tensile load there is strain incompatibility among its materials and the Stage I response is a lot stiffer than experimentally evaluated stress strain curves. Therefore, the stress strain curves of RC elements subjected to tension lies between the bare bar curve and Stage I curve. Tension stiffening is the difference between two strains, ε_m and ε_{m2}, for a given external load N. For the same load, the difference between strains ε_m and ε_{m1} represents strain incompatibility. *Fantilli et al.* [18].

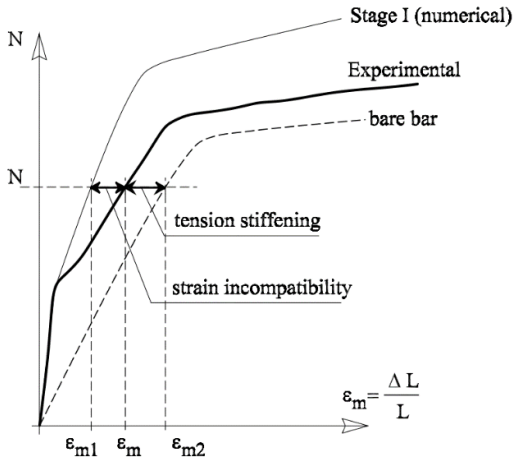

Figure 16: Experimental and numerical N-εm curves of the element tested in tension

4.2 Possible model

If we want to use HPFRCC as pavement we can model the concrete pavement and the soil; soil is similar to the steel in RCC structures, as a Stage I cross section where whole cross section will contribute against external actions. The external action in concrete soil interaction after casting concrete is just the shrinkage. We can consider this reduction in volume as an imposed strain, which is applied as a constant value on the concrete, and a perfect interaction between concrete and soil. If we know the geometric and mechanical properties of concrete, we can define the state of stress and strain by using Colonnetti's theory of elastic coaction.

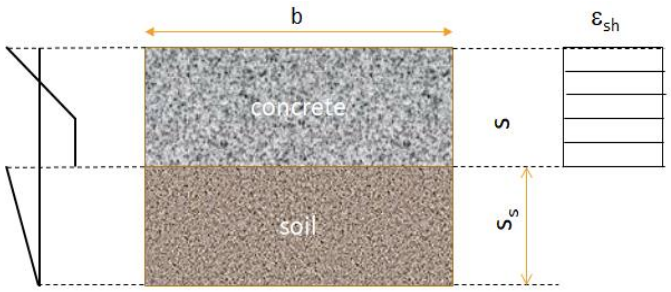

Figure 17: A Composite concrete and soil model

In RCC structures during the shrinkage phenomena the concrete closer to the steel is in tension and the steel is in compression. As shown in figure due to a restrain closer to the surface of the soil the part of concrete at the interface is in tension and soil is in compression. We need a model for the calculation of stresses and strains and finding the strain to be lower than the strain that causes localization. Before using the model we need the mechanical properties of concrete for which we need to test materials at different stages of curing, 1d, 3d, 7d up till 28d, as the shrinkage and mechanical properties of concrete are changing with time. The stress strain relationship of materials will be defined by performing Direct Tensile test and also with the Three Point Bending test. As direct tensile test is difficult to perform by companies because of high cost so it will be corelated with the bending test which are easier to perform.

Three types of parameters required for the model are:

1. Geometrical properties of concrete and soil.
2. Mechanical properties of concrete.
3. Mechanical properties of soil.

Table 4: Geometrical properties of composite section

Geometrical properties		
Width	b =	200
Depth	S =	200
Soil thickness	Ss =	102

Table 5: Mechanical properties of concrete

Mechanical properties of concrete		
Shrink strain (negative)	ε_{sh} =	-0.004
Elastic modul	Ec =	30000
Cracking strength	f_{ct} =	3
Ultimate strength	f_u =	4
Maximum tens. strain	ε_u =	0.002
Compressive strength	f_c =	30
Maximum comp. strain (negative)	ε_{cu} =	-0.001

Table 6: Mechanical properties of soil

Mechanical properties of soil		
elastic modulus surf.	Et_0 =	3000
variation of Es	K_t =	3
average elastic modulus	E_t =	3153

4.2.1 Soil parameters

The elastic modlus of soil E_s is not constant and increases with depth of soil. At the surface we have E_{t0} and going down it will change with the variation K_t ; in the end the average elastic modulus E_t is considered.

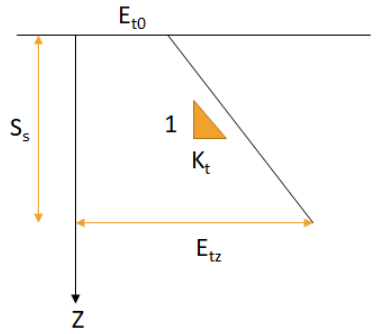

Figure 18: Variation of soil modulus with depth

$$E_{tz} = E_{t0}K_t.z$$

$$E_{tz} = E_{t0}K_t.S_s$$

$$E_t = \frac{E_{t0} + E_{tz}}{2}$$

$$E_t = E_{t0} + \frac{K_t.S_s}{2}$$

4.2.2 Position of centroid

As we are in the theory of elastic coaction, the first step is to define an elastic modulus as a refernce modulus for the materials: it is considered as E_0. In our case we consider the refernce modulus of concrete as a reference value $E_0 = E_c$. A_0 is the homogeneous area and the homogenization should be practiced in the whole cross-section (shown in Figure 19).

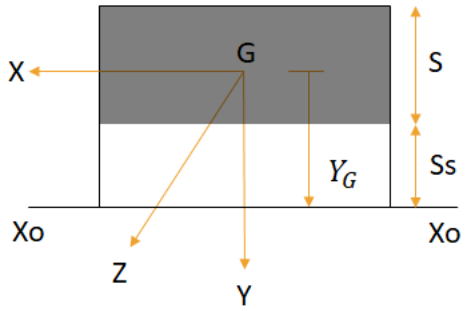

Figure 19: Position of centroid of a composite section

$$E_0 = E_c$$

$$A_0 = \frac{E_c}{E_0}.s.b + \frac{E_t}{E_0}.S_s.b$$

$$A_0 = s.b + \frac{E_t}{E_c}.S_s.b$$

Position of centroid Y_G can be found as:

$$Y_G = \frac{S_{x0}}{A_0}$$

where,

$$S_{x0} = \frac{E_c}{E_c}.b.s\left(\frac{S}{2} + S_s\right) + \frac{E_t}{E_c}.b.S_s.\frac{S_s}{2}$$

$$S_{x0} = b.s\left(\frac{S}{2} + S_s\right) + \frac{E_t}{E_c}.b.\frac{{S_s}^2}{2}$$

$$Ix_0 = \left[\frac{bS^3}{12} + b.S\left(\frac{S}{2} + S_s - Y_G\right)^2\right] + \left[\frac{b{S_s}^3}{12} + b.S_s\left(\frac{S_s}{2} - Y_G\right)^2\right]\frac{E_t}{E_c}$$

4.2.3 State of stress

State of stress, which is orthogonal to the direction considered (z direction), is given by:

$$\sigma_z = E(\lambda + \mu x.y - \varepsilon_{sh})$$

where shrinkage strain is subtracted from concrete slab only.

$$\lambda_{tot} = \lambda_{el} + \bar{\lambda}$$

As λ_{el} (elastic) is zero, so only remaining is $\bar{\lambda}$, which is due to imposed strain.

$$\lambda_{tot} = \bar{\lambda} = \frac{1}{A_0}\int_{Ac}\frac{E_c}{E_c}.\varepsilon_{sh}.dA$$

$$\bar{\lambda} = \frac{\varepsilon_{sh}}{A_0}.b.s$$

Also, $\mu_{xtot} = \mu_{xel} + \bar{\mu}x$ and μ_{xel} (elastic) is zero.

$$\mu_x = \bar{\mu}_x = \frac{1}{I_{x0}}\int_{Ac}\frac{E_c}{E_c}\varepsilon_{sh}.y.dA$$

$$\bar{\mu}_x = \frac{\varepsilon_{sh}}{I_{x0}}\int_{Ac} y\,.dA$$

where, $\int_{Ac} y\,.dA$ represents the static moment of the concrete part with respect to G:

$$S_{xG} = b.S\left(-\frac{S}{2} - S_s + Y_G\right)$$

So finally the total stress and strain will be

$$\varepsilon_{tot} = \bar{\lambda} + \bar{\mu}_x.y - \varepsilon_{sh} \quad (9)$$

$$\sigma_z = \begin{cases}\sigma_c \\ \sigma_s\end{cases} \quad (10)$$

$$\sigma_c = E_c\left(\bar{\lambda} + \bar{\mu}x.y - \varepsilon_{sh}\right)$$

$$\sigma_s = E_t\left(\bar{\lambda} + \bar{\mu}x.y\right)$$

This procedure can be used when both materials, concrete and soil, behave in the linear elastic regime. Although it is not true for the case of concrete where the stress strain behavior is non linear, this procedure needs to be modified for non linearity of the material. When we enter the stress strain relationship with a given ε we are finding the stress σ_E but it is not real, the real is σ_R so we over-estimate the state of stress because we are considering linear elastic behavior but on contrary it is non linear behavior.

If we want to maintain the linear elastic approach, we have to translate the linear curve to the non linear curve, so we need the translation of the origin at a value of new non linear imposed strain ε_{nl}. In other words, the effect of non linearity is a new imposed strain.

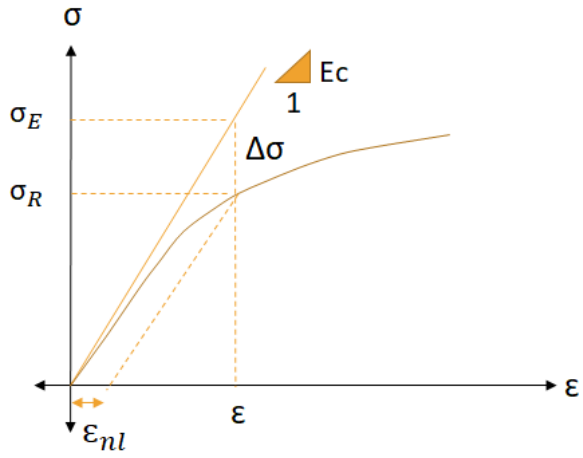

Figure 20: Imposed strain due to non-linearity

The real state of stress σ_R in that case is given by;

$$\sigma_R = E(\varepsilon - \varepsilon_{nl})$$

$$\varepsilon_{nl} = \frac{\sigma_E - \sigma_R}{E}$$

$$\varepsilon_{nl} = \frac{E\varepsilon - \sigma(\varepsilon)}{E} \quad (11)$$

$$\varepsilon_T = \varepsilon_{sh} + \varepsilon_{nl} \quad (12)$$

The above mentioned approach is to be used for concrete, but we can extend it to soil as well. New increment of imposed λ and μ can be written as:

$$\Delta\bar{\lambda} = \frac{1}{A_0}\int \frac{E}{E_0}.\varepsilon_T dA \quad (13)$$

$$\Delta\bar{\mu}_x = \frac{1}{I_{x0}}\int \frac{E}{E_0}.\varepsilon_T.ydA \quad (14)$$

New imposed strain parameters can be computed

$$\bar{\lambda} = \bar{\lambda} + \Delta\bar{\lambda} \quad (15)$$

$$\bar{\mu}_x = \bar{\mu}_x + \Delta\bar{\mu}_x \quad (16)$$

Finally the new state of stress is:

$$\sigma = E\left(\bar{\lambda} + \bar{\mu}x.y - \varepsilon_T\right) \quad (17)$$

We enter stress strain relationship with a new strain found from equation 12, and obtain another σ_E; but the real was σ_R, so another translation will be required with a value $\Delta\varepsilon_{nl}$. This new $\Delta\varepsilon_{nl}$ will be applied to the whole cross section as before.

$$\bar{\varepsilon}_T = \varepsilon_T + \Delta\varepsilon_{nl} \quad (18)$$

After this we put equation 18 in equations 13 and 14 to repeat the steps to find σ from equation 17. This iteration will stop when the difference between consecutive values of $\Delta\varepsilon_{nl}$ is mathematically zero.

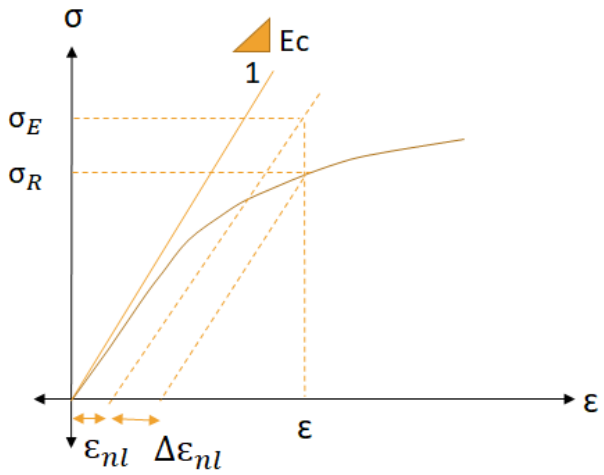

Figure 21: Iteration of imposed strain due to non-linearity

The aforementioned procedure can be converted into an excel macro and the results obtained can be shown in Figure 22.

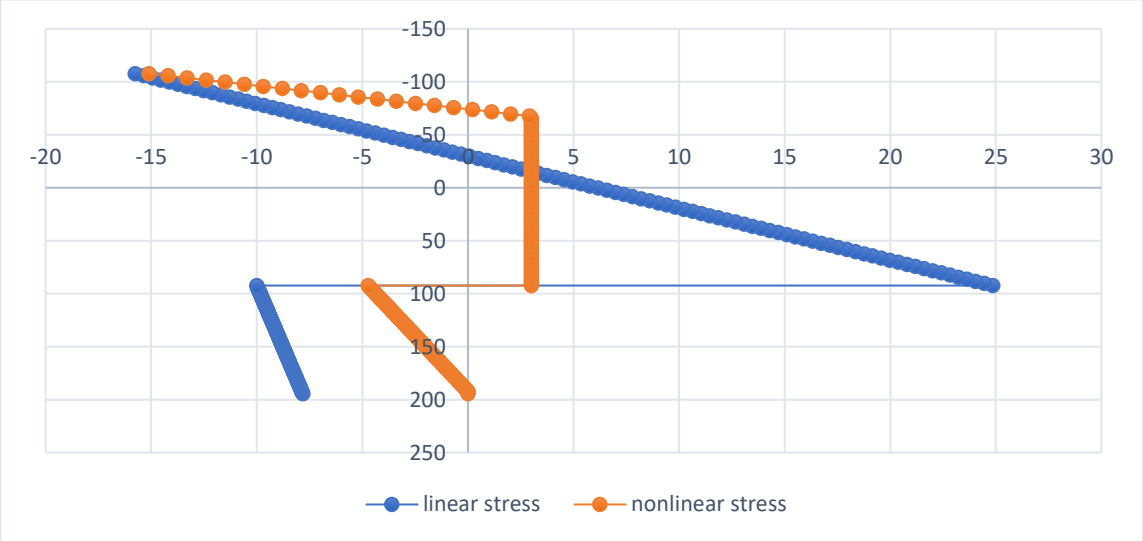

Figure 22: State of stress in the composite

As we consider the nonlinear stresses, we must keep in mind that the thickness of soil layer Ss is unknown. The value we introduced in the beginning was only a trial value as in Ss, where the average elastic modulus is computed, tensile stresses are not allowed. Thus, the above procedure should be repeated by changing Ss until the state of stress in the bottom part of Ss is zero. In other words, only compressive stresses must be present in the soil.

The limit to the crack width or the maximum tensile strain allowed for the jointless slab, total strain from equation 19 must be considered which is represented as epstot in Figure 23. While the brown curve is of the pseudo elastic strain, eps_pseudo el, coming from equation 20. Soil does not have imposed strain so for the soil layer pseudo elastic strain and the total strain are the same. The blue vertical line shows the maximum tensile strain limit, and for jointless slab without a crack, the pseudo elastic strain must be lower than this limit. As shown in Figure 23, the imposed strain will result in cracking of the slab, as it crossed the maximum tensile strain limit:

$$\bar{\lambda} + \bar{\mu}_x . y \tag{19}$$

$$\left(\bar{\lambda} + \bar{\mu}x . y - \varepsilon_T\right) \tag{20}$$

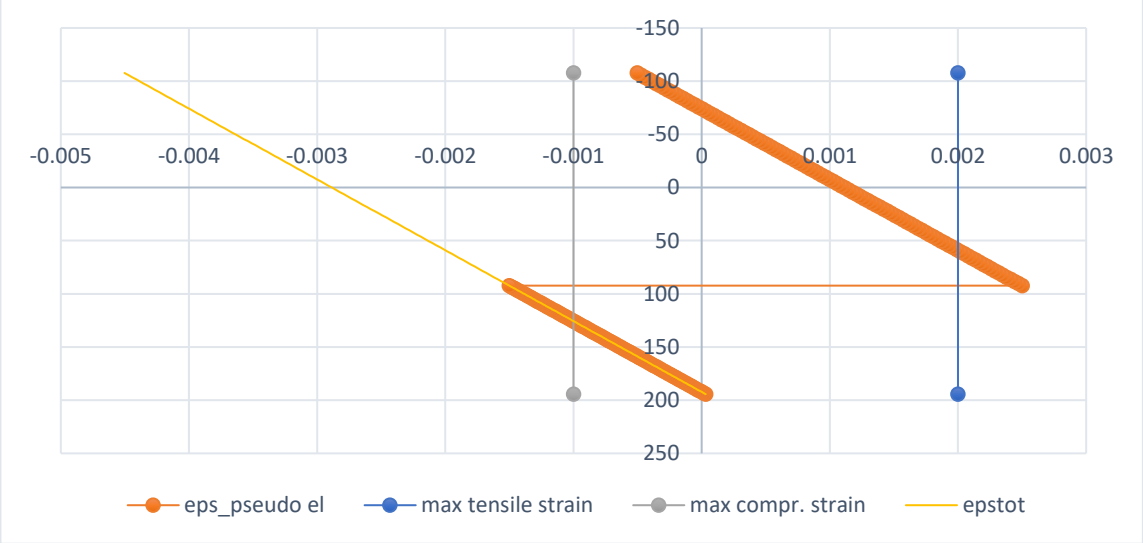

Figure 23: Total strain and maximum tensile strain limit

5. Numerical analysis

Concrete performance is a measure of its mechanical properties which include compressive strength, tensile strength, modulus of elasticity, shrinkage, creep, and flexural strength. Concrete behavior in its early age is a representative of its long-term properties and performance. The appropriate mix selection and mix proportions is fundamental for high strength and durable concrete production and without proper attention in its early age there could be a loss in its mechanical properties.

5.1 Concrete properties with time

Since concrete is an aging material, its mechanical properties depend on the rate of hydration of its microstructure at an early stage and the rate of development is different for each mechanical property.

The compressive strength of concrete is the indication of its quality and is the fundamental concrete property. At an early age the rate of development of compressive strength is much higher than the rate at later ages. Most important factors involving the gain in compressive strength of concrete are the type of cement, water to cement ratio, admixtures and curing conditions of concrete. For a given water to cement ratio, higher hydration rate gives higher strength in early age of concrete [19]. Tensile strength in concretes early age is a key property and provides a major role in resisting early age cracking that effects the structure stiffness, thermal stresses, shrinkage. As the concrete is in plastic stage in its early age, it is difficult to measure its tensile properties. Tensile strength and compressive strength development are also affected by such factors as the tensile strength of concrete is in a relationship with its compressive strength. The relationship between both strengths is influenced by concrete age, type of aggregates, concrete curing conditions. Concretes tensile strength gain is more rapid than its compressive strength gain in early ages [20]. The tensile strength as a function of its compressive strength is given by Neville, 1996.

$$f_t = k(f_c)^n$$

Where f_c is the concretes compressive strength and k, n are relation coefficients which are given in Table.7 of ACI, 2005. The tensile strain capacity of concrete before its initial setting is very high because of its plastic nature, once the initial setting starts tensile strain capacity tends to decrease [21].

Main cause of concrete cracking which leads to the loss of durability and serviceability of concrete is the shrinkage. Shrinkage can be categorized into two types: Drying shrinkage and autogenous shrinkage. There is not a specific relationship between the magnitudes of both shrinkages, but the value of early age shrinkage might exceed its long term shrinkage due to the rapid drying conditions. Concrete is much sensitive to its internal stresses because of low strength and low strain capacity in its early age. For this reason, any induced stress which exceeds the concrete tensile strength will result in cracking, either microscopic which can start increasing into macroscopic later on or with already enough crack widths comparable to the aged cracking. Several parameters which affect the early age concrete shrinkage are [22];

- Binder type, binder content and rate of hydration.
- The aggregate content.
- Water content.
- Admixtures.
- Curing conditions.

5.2 Prediction models

Concrete properties evolve with time as the hydration continues starting from the low strength at early age up to high strength in old age. Different models are described in the codes as well as different researchers for estimating the compressive stress and strain, tensile stress and strain, shrinkage strain, creep and modulus of elasticity. Out of simple models described by different researchers a well-known equation is given by Neville,2003 for estimating ultimate shrinkage at any given time.

$$s(t) = \frac{t}{t + 35} . S_{ult} \qquad (21)$$

where,

$s(t)$ = shrinkage after t days from the end of 7-day moist curing.

S_{ult} = ultimate shrinkage.

t = time from the end of moist curing (days).

5.2.1 Compressive strength model

Concrete compressive strength at any age t depends on the cement type, curing conditions, and temperature. Concretes compressive strength at various ages $f_{cm}(t)$ with curing conditions according to code EN 12390, mean temperature of 20°C can be obtained from expressions given by Eurocode 2.

$$f_{cm}(t) = \beta_{cc}(t) f_{cm} \tag{22}$$

where,

$$\beta_{cc}(t) = exp\left\{s\left[1 - \left(\frac{28}{t}\right)^{1/2}\right]\right\} \tag{23}$$

where,

$f_{cm}(t)$ = Mean compressive strength at an age t day.

f_{cm} = 28 day mean compressive strength.

$\beta_{cc}(t)$ = Coefficient depending on concrete age t.

t = Concrete age in days.

s = Coefficient depending on cement type (0.2, 025, 0.38).

5.2.2 Tensile strength model

Tensile strength development with time is affected by size of structural member, drying and curing condition. Tensile strength approximation $f_{ctm}(t)$ in time is given by Eurocode 2 and is equal to:

$$f_{ctm}(t) = \left(\beta_{cc}(t)\right)^{\alpha} . f_{ctm} \tag{24}$$

where,

$$\beta_{cc}(t) = exp\left\{s\left[1 - \left(\frac{28}{t}\right)^{1/2}\right]\right\} \tag{25}$$

$$f_{ctm} = 0.3 f_{ck}^{2/3} \qquad \leq C50/60 \qquad (26)$$

$$f_{ctm} = 2.12\, ln\left(1 + \left(f_{cm}/10\right)\right) \qquad > C50/60 \qquad (27)$$

α = 1 for t < 28

α = 2/3 for t ≥ 28

5.2.3 Modulus of Elasticity

The modulus of elasticity of concrete (Ec) is the ratio of the applied stress and the strain corresponding to that stress. It shows concrete ability to withstand deformation and stiffness against the applied load.

Variation of the modulus of elasticity with time can be estimated by:

$$E_{cm}(t) = \left(f_{cm}(t)/f_{cm}\right)^{0.3} E_{cm} \qquad (28)$$

where, $E_{cm}(t)$ and $f_{cm}(t)$ represents modulus and strength at an age of t days and E_{cm} and f_{cm} are the 28 days modulus and strength. The relation between $f_{cm}(t)$ and f_{cm} can be obtained from equation 22.

5.2.4 Tensile strain

Deformation of a body due to the application of tensile stress is known as tensile strain. It is a dimensionless quantity which is just a ratio of change in length to the original length of an object. The tensile strain generally increases with time and the prediction model for finding the tensile strain can be indirectly found from Eurocode 2 using the tensile stress and modulus of elasticity predictions with time as

$$\varepsilon = \sigma/E$$

5.2.5 Shrinkage model

Two types of strains, dry shrinkage and autogenous shrinkage strain combines to represent the total shrinkage strain in an object. Migration of water through the hardening of concrete makes the dry shrinkage strain development a slow process. Hardening of concrete which develops in early days after concrete casting results in major part of autogenous shrinkage and is a linear function of the concrete strength.

Total shrinkage strain ε_{cs} can be represented as a sum of dry shrinkage and autogenous shrinkage strain as given by

$$\varepsilon_{cs} = \varepsilon_{cd} + \varepsilon_{ca} \tag{29}$$

where,

ε_{cs} = total shrinkage strain

ε_{cd} = dry shrinkage strain

ε_{ca} = autogenous shrinkage strain

Drying shrinkage strain development in time is given by Eurocode 2 by the following expression:

$$\varepsilon_{cd}(t) = \beta_{ds}(t, t_s).\, k_h.\, \varepsilon_{cd,0} \tag{30}$$

where,

k_h = coefficient which depend on the notional size h_o

h_0	k_h
100	1.0
200	0.85
300	0.75
≥ 500	0.70

$$\varepsilon_{cd,o} = 0.85\left[(220 + 110 * \alpha_{ds1}) * exp\left(-\alpha_{ds2}\frac{f_{cm}}{f_{cmo}}\right)\right] * 10^{-6} * \beta_{RH} \tag{31}$$

$$\beta_{RH} = 1.55\left[1 - \left(\frac{RH}{RH_o}\right)^3\right] \tag{32}$$

where,

fcm = mean compressive strength (MPa)

fcmo = 10 Mpa

α_{ds1} = coefficient depending on cement type

= 3 for Class S cement

= 4 for Class *N* cement

= 6 for Class *R* cement

α_{ds2} = coefficient depending on cement type

= 0,13 for Class S cement

= 0,12 for Class *N* cement

= 0, 11 for Class *R* cement

RH = ambient relative humidity (%)

RHo = 100%

and

$$\beta_{ds}(t, t_s) = \frac{(t - t_s)}{(t - t_s) + 0.04\sqrt{h_o{}^3}} \qquad (33)$$

where,

t = concrete age considered at the moment, in days.

t_s =concrete age at the beginning of dry shrinkage (days).

h_o = notional size of the cross section in mm.

$$h_o = {}^{2A_c}/_{u} \qquad (34)$$

where,

Ac = concrete cross-sectional area, *u* = perimeter of that part of the cross section which is exposed to drying.

Below are the Nominal unrestrained dry shrinkage values $\varepsilon_{cd,0}$ (in ${}^{0}/_{00}$) for concrete of cement CEM Class N

$f_{ck}/f_{ck,cube}$ (MPa)	Relative Humidity (in $^0/_0$)					
	20	40	60	80	90	100
20/25	0.62	0.58	0.49	0.30	0.17	0.00
40/50	0.48	0.46	0.38	0.24	0.13	0.00
60/75	0.38	0.36	0.30	0.19	0.10	0.00
80/95	0.30	0.28	0.24	0.15	0.08	0.00
90/105	0.27	0.25	0.21	0.13	0.07	0.00

The autogenous shrinkage strain is given by:

$$\varepsilon_{ca}(t) = \beta_{as}(t)\varepsilon_{ca}(\infty) \tag{35}$$

where,

$$\varepsilon_{ca}(\infty) = 2.5\ (f_{ck} - 10)10^{-6} \tag{36}$$

and

$$\beta_{as}(t) = 1 - exp(-0.2t^{0.5}) \tag{37}$$

Where t is given in days.

For the structural analysis of concrete members, only dry shrinkage and autogenous shrinkage are taken into account. Figure 24 shows the ratio between both, drying shrinkage and autogenous shrinkage components, *Gribniak et al.* 2008 [23]. For the normal strength concretes where autogenous shrinkage strain takes only 10 to 20 percent of total shrinkage strain there is no specific distinction of autogenous shrinkage strains from the drying shrinkage strains. For the case of high strength concretes, both shrinkage strains should be treated separately because with the age of concrete there is a big variation between the ratio of these strains to the total shrinkage strains.

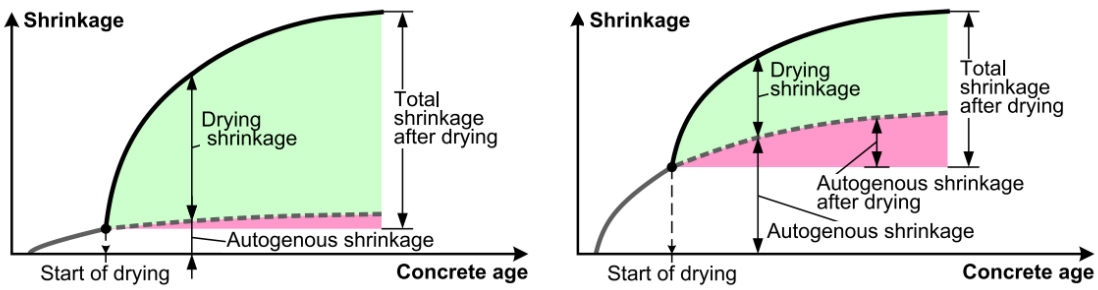

Figure 24: Shrinkage strain components in normal (left) and high-strength (right) concrete

For high strength concretes made with low water to cement ratio and silica fumes, major portion of total shrinkage strains is represented by autogenous shrinkage strains with respect to drying shrinkage strains. *Zhang et al*. [24]. Addition of silica fumes for high strength concretes and reducing the water cement ratio results in reduction of drying shrinkage strain because of the fact that silica fumes densifies the hydrated cement paste resulting in slow water evaporation hence less drying shrinkage. *Yoo et al*. [25] studied three samples of ultra-high strength concrete, the sample with the highest W/B ratio caused more drying shrinkage than the other samples because due the relative difference in humidity higher amount of pore water in the hardened cement paste causes more water evaporation into the atmosphere which results in higher dry shrinkage.

As this thesis study is focused on drying shrinkage of HPFRCC, only the drying shrinkage prediction models given by different researchers will be discussed. The Eurocode (EC2, already discussed), for ACI 209R-92 model and Ross model, the experimentally measured 147 days dry shrinkage was used as the ultimate drying shrinkage value for the drying shrinkage prediction; For Bazant–Baweja B3 model and Gardner model, the ultimate drying shrinkage was found by the equations presented by the Bazant–Baweja B3 model and Gardner model respectively. *Gardner and Lockman* [26] provided a model (GL-2000) suitable for conventional concrete with a 28 days compressive strength up to 82 MPa and water to cement between 0.4 to 0.6. The model does not take into account the effects of admixtures, additives, curing methods, and casting temperature.

Drying shrinkage strain model proposed by Bazant and Baweja is one of the most used models currently. B3 model developed by *Bazant and Baweja* [27] is a mathematical model considering different phenomena like creep and shrinkage with time. B3 model's coefficient of variation is very low in comparison to ACI209R and EN1992 models, stated by Bazant and Baweja. To reduce the risk of error because of inaccurate value associated with elastic modulus, B3 model uses the compliance function. Drying shrinkage strain prediction equation proposed by B3 model is given as:

$$\varepsilon_{sh}(t, t_o) = \varepsilon_{sh\infty} * k_h * tanh\sqrt{\frac{t - t_o}{\tau_{sh}}} \qquad (38)$$

$$\varepsilon_{sh\infty} = -\alpha_1 * \alpha_2[1.9 * 10^{-2} * w^{2.1} * (f_c')^{-0.28} + 270] * \frac{\left(\frac{607}{4 + 8.5 * 607}\right)^{1/2}}{\left(\frac{t_o + \tau_{sh}}{4 + 8.5 * (t_o + \tau_{sh})}\right)^{1/2}} \quad (39)$$

$$k_h = 1 - h^3 \quad (40)$$

$$\tau_{sh} = k_t(k_s D)^2 \quad (41)$$

where, $D = {2v}/{S}$ (*v/s* is the *volume to surface* ratio of concrete member in mm), k_s can be assumed 1, and

$$k_t = 8.5 t_0^{-0.08} f_c^{-0.25} \quad (42)$$

where,

ε_{sh} = Dry shrinkage strain,

$\varepsilon_{sh\infty}$ = Ultimate shrinkage strain (in 10^{-6}),

t = Concrete age (days),

to = Concrete age at the start of drying (days),

α_1 = Cement type factor (1.1 for type III cement),

α_2 = Curing factor (1.2 for normal curing in air),

w = Water content (kg/m^3),

f'$_c$ = 28-day concrete compressive strength (MPa),

k_h = Humidity factor (if humidity = 70%, h=0.7),

τ_{sh} = Shape and size factor.

5.3 Numerical analysis and results

As discussed earlier that the state of stress and strain in concrete changes with time as so the drying shrinkage strain, the imposed strain, the numerical analysis is required to find

the minimum slab thickness in order to avoid cracking in the slab. The procedure to find the minimum slab thickness is to compare the maximum state of stress produced by the imposed strain at different times with the strength of UHPFRCC, maximum allowed strains by the concrete at different times. The maximum state of stress can be found from the possible model described in section 4.2 of this thesis while the maximum allowable strains can be taken from the literature or also from the tensile strain prediction model from Eurocode 2 as described in section 5.2.4 of this thesis.

While comparing both the strains at the same time, there can be a time in which the maximum state of stress produced by the imposed strain can be larger than the concrete strain capacity. At that time there will be a crack in the slab for a given geometrical and mechanical properties and to avoid that crack we must change the thickness of the slab.

Analysis starts with finding the drying shrinkage strains at different times starting from one hour after casting up till 28 days. The prediction model used in this thesis is the model given by Eurocode 2, which is already discussed, using equation 19. Starting from 1 hour up till 28 days, the drying shrinkage strains are computed. The parameters used in the model and the shrinkage strains obtained as a result with respect to time are shown below:

	humidity	0.7		thickness =	50	mm
	fc =	30	Mpa	width =	10000	mm
	β_{RH}	1.01835		Ac (cross sectional area)=	500000	mm2
	$\varepsilon_{cd,o}$	0.00039858		u (surface perimeter) =	10000	mm
	kh =	1		ho =	100	mm
	to =	0.04166667	days			
hours	days	β_{ds}	εsh			
1	0.04166667	0	0			
2	0.08333333	0.00104058	-4.148E-07			
3	0.125	0.002079	-8.286E-07			
4	0.16666667	0.00311526	-1.242E-06			
5	0.20833333	0.00414938	-1.654E-06			
6	0.25	0.00518135	-2.065E-06			
7	0.29166667	0.00621118	-2.476E-06			
8	0.33333333	0.00723888	-2.885E-06			
9	0.375	0.00826446	-3.294E-06			
10	0.41666667	0.00928793	-3.702E-06			
11	0.45833333	0.01030928	-4.109E-06			
12	0.5	0.01132853	-4.515E-06			

Figure 25: Parameters for shrinkage model

Figure 26: Drying shrinkage with time

The trend shows, as the time increases the drying shrinkage increases.

Now the drying shrinkage obtained are used as imposed strains in the model to predict the state of stress and strain against these imposed shrinkage strains.

geometrical properties				mechanical properties of concrete			mechanical properties of soil		
width	b=	10000		shrink strain (negative)	erit=	-1.64E-04	elastic modulus surf.	Et0=	3000
depth	s=	50		Elastic modul	Ec=	30000	variation of Es	kt=	3
soil thickness	st=	65.7		cracking strength	fct=	3			
				ultimate strength	fu=	4	average elastic modulus	Et=	3098.55
				maximum tens. strain	eu=	0.002			
				compressive strength	fc=	30			
				maximum comp. strain	euc=	-0.001			

Figure 27: Parameters of stress strain model

To use the model, the soil thickness needs to be defined first so that there are no tensile stresses in the soil but only the compressive stress. A code was introduced in the macro to automate the soil thickness considering the initial thickness provided as a start then it calculates the state of stress with each increment of the soil thickness provided for iteration until it finds all the negative values as state of stress in the soil. Hence, only the soil in

compression is considered as in tension the soil is not good. This selection of soil thickness is important as it is the key factor for calculating the average elastic modulus of soil.

With all the parameters, the state of stress and strain can be found against imposed shrinkage strains, as shown below:

signl	eps_pseudo el	epstot		maximum tensile strain	
2.03716E-15	1.6795E-07	1.6795E-07		y	epsu
-0.00299175	-9.65531E-07	-9.65531E-07		83.7870081	0.002
-0.00650389	-2.09901E-06	-2.09901E-06		-31.912992	0.002
-0.01001604	-3.23249E-06	-3.23249E-06			
-0.01352819	-4.36597E-06	-4.36597E-06			

Figure 28: Non-linear stress and strains from model

These values are nonlinear stresses, nonlinear pseudo elastic strains and total strains respectively, in the end the maximum tensile strain limits are added to know if pseudo elastic strains cross them then there is a crack at that imposed strain. Figure 29 shows a better picture where maximum tensile strain (5.07998E-05 in this case) in the concrete will be required to compare with the strength of concrete.

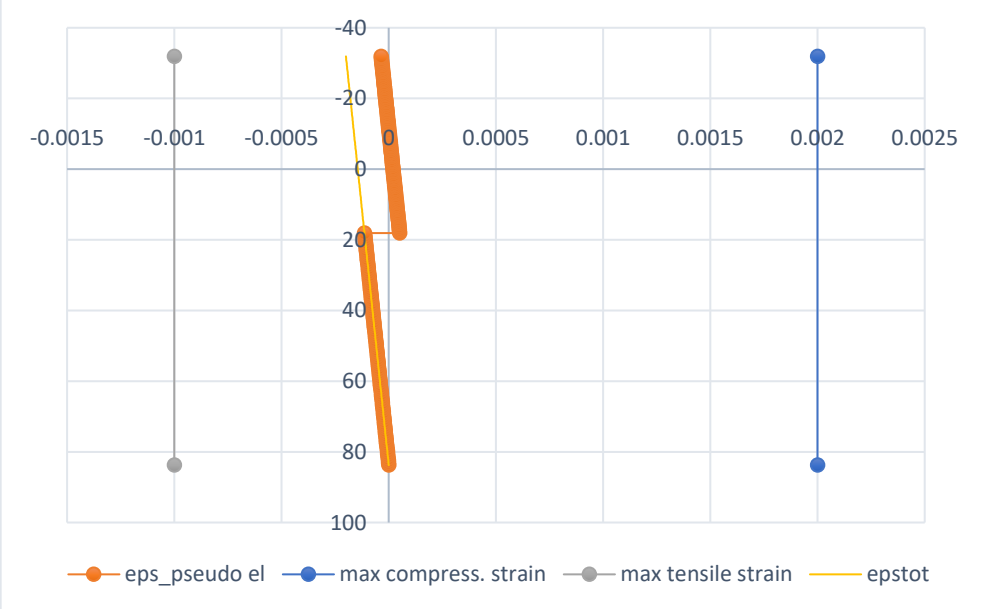

Figure 29: Maximum tensile strains

Performing the same analysis for a selected width of slab 10m and keeping all other parameters same except changing imposed shrinkage strain with time the maximum shrinkage strains are computed. This is done for a slab of different thicknesses, 50mm and 80mm. The plot for both thicknesses is shown in Figure 30.

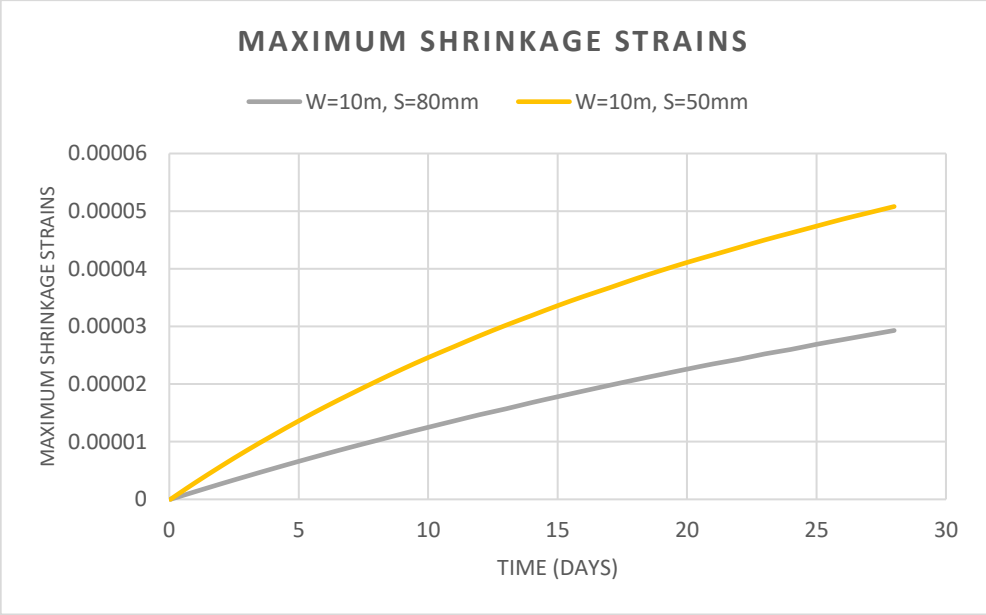

Figure 30: Maximum shrinkage strains

The maximum shrinkage strains for a thicker slab are lower than the maximum shrinkage strains for a thinner slab, means as the slab thickness increases the maximum drying shrinkage decreases. This trend corelates with the experimental results found in literature. Y. Ohama and S. Kan prepared various sized specimen of polymer-modified concrete with different mix proportions for drying shrinkage and compressive strength evaluations at different curing conditions. Test results indicated that irrespective of polymer-cement ratio, with an increase in specimen size the drying shrinkage decreases while with a decrease in specimen size the compressive strength increases. [28].

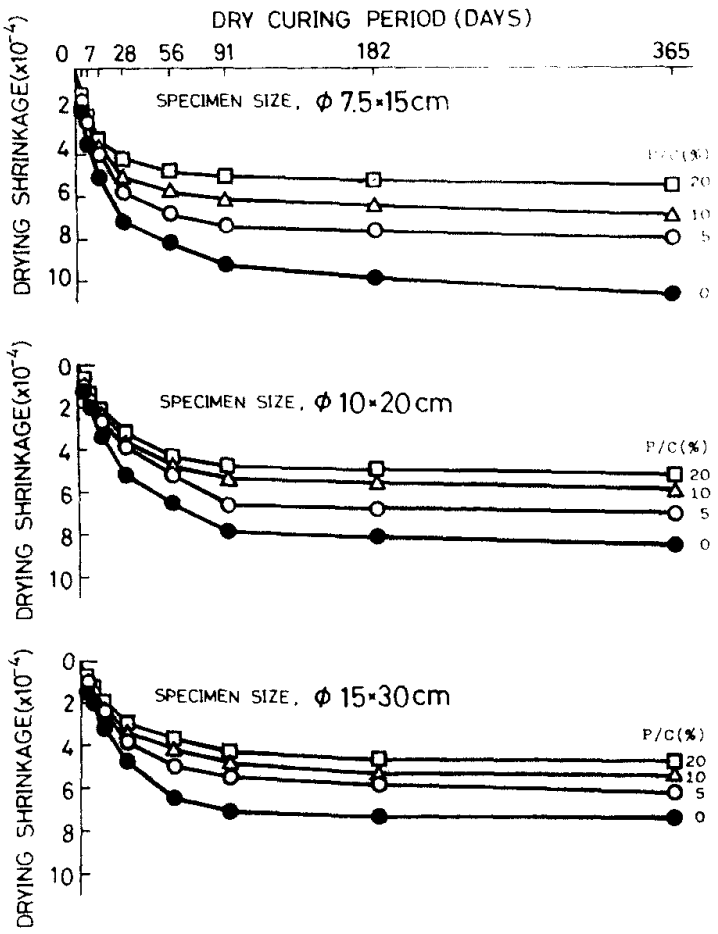

Figure 31: Specimen size vs drying shrinkage strains

Lenka and Petr [29] evaluated the effect of specimen size on concretes ultimate drying shrinkage. They analyzed the experimental data and compared them with the codes in practice, namely the Eurocode 2 and ACI 209.2R-08 and found that by increasing the effective thickness of specimen the drying shrinkage decreases. The ultimate drying shrinkage strains with different specimen sizes are compared in Figure 32.

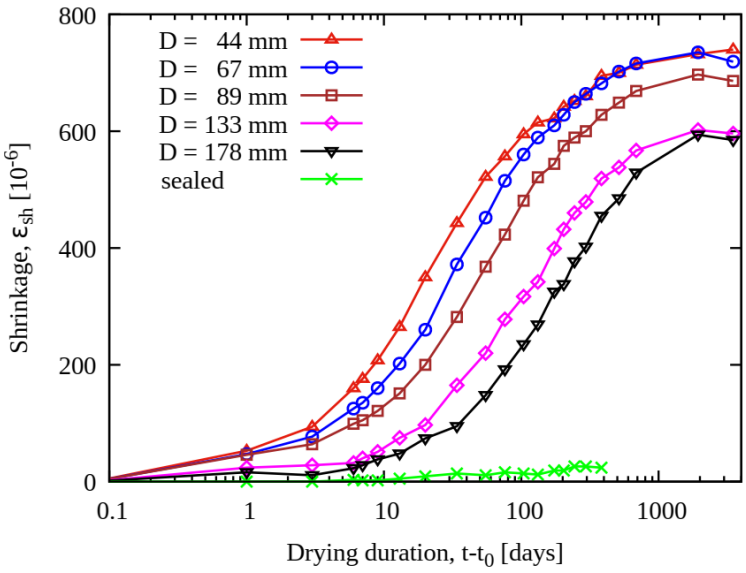

Figure 32: Drying Shrinkage variation with specimen size

For the experimental data of maximum concrete strains there is quite less work in literature on early age concrete strains because of increasing difficulty in the application of the tensile load on a concrete specimen and the complications of measuring strains in the plastic concrete. Boshoff [30] conducted direct tensile test on plastic concrete. The molds used earlier were not as adequate for accurately measuring the tensile strains so based on the previous researches a new dog-bone shaped mold supported on an air bearing was proposed by Boshoff and the boundary conditions were a compromise between freely rotating and fully fixed. For all the tests a conventional concrete mix with a 28 days cubic compressive strength of 37.5 MPa, slumps of 7cm was used which is also suitable for slabs.

The strain results of the concrete specimen showed the strain capacity (ε_{cap}) between 0.2 and 0.3 percent elongation for the first three hours, which is high. The strain capacity decreased significantly to around 0.067 percent elongation within one hour between initial and final setting times and continues to decrease to around 0.027 percent elongation at fifth hour, then at sixth hour it slightly increases to 0.035 percent. Between the initial and final setting times this significant and sudden decrease of strain capacity means that there is a sudden change from concretes ductile behavior to brittle behavior where in ductile

behavior the material that can withstand large deformations before it cracks and in brittle behavior cracking occurs at much lower deformation. Plastic shrinkage between initial and final setting time of concrete is a result of sudden drop in its strain capacity.

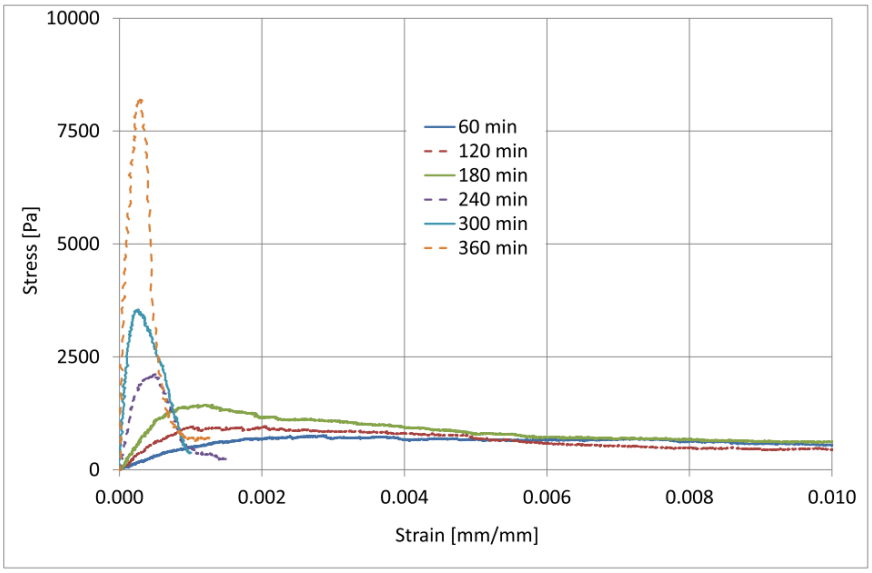

Figure 33: Typical stress strain curves at 1 h intervals up to 6 h

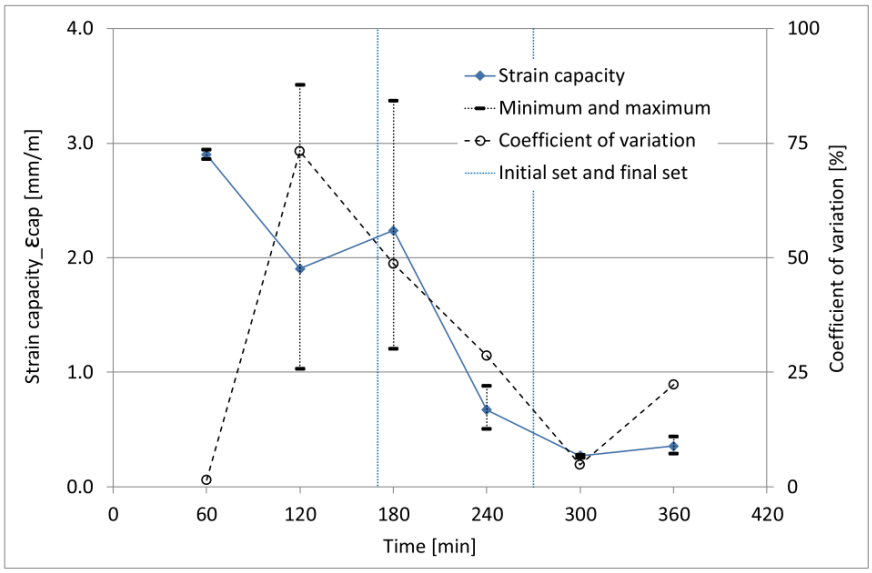

Figure 34: Strain capacity development

Another study was conducted by Hammer [31] in which stresses and strains of plastic concrete at the age up till 11 hours has been found. These results also showed that the plastic concretes strain capacity is high in the beginning and then it starts decreasing. The stress strain relations can be seen in the Figure 35 and Figure 36.

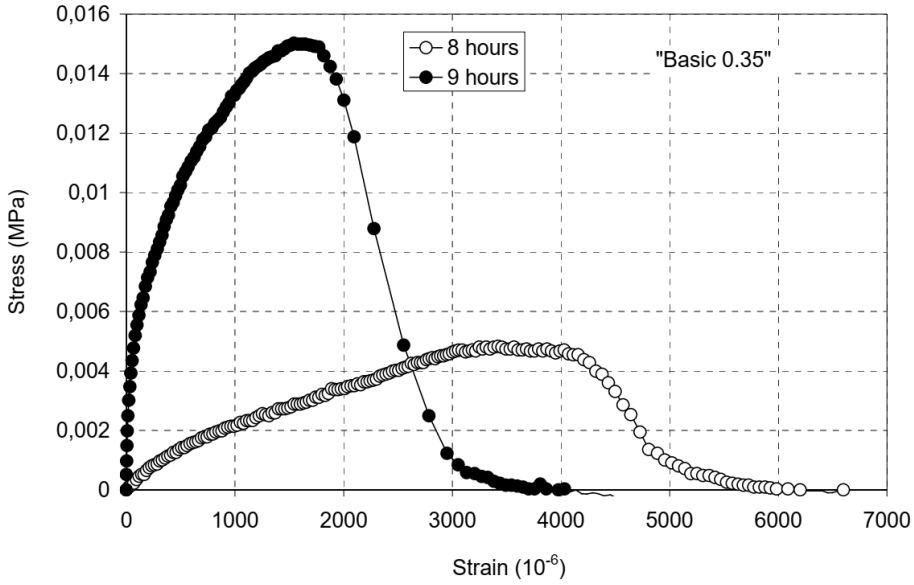

Figure 35: Tensile stress strain at the age of 8 and 9 hours

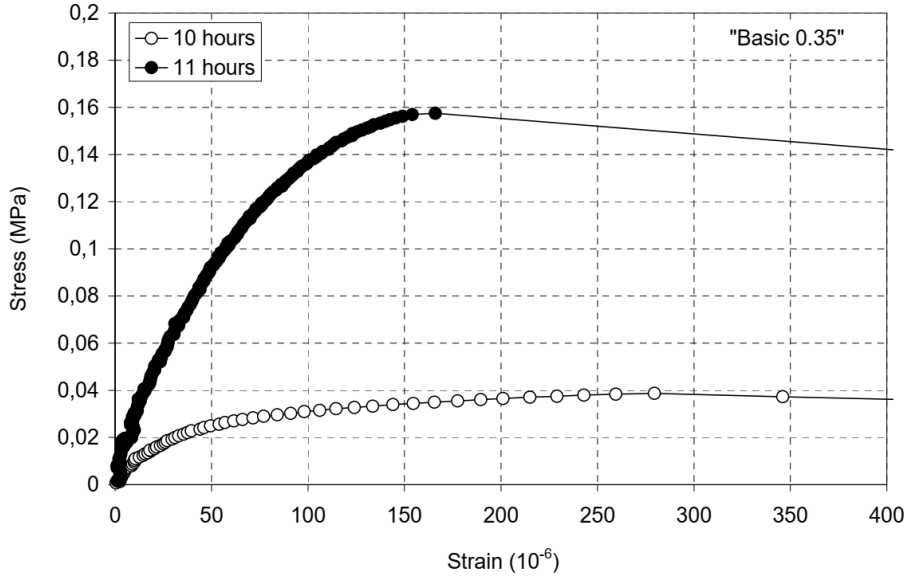

Figure 36: Tensile stress strain at the age of 10 and 11 hours

Furthermore Loukili et al. [32] performed direct tensile tests on two sets of concrete at the ages of 7, 10, 15, 20 and 24h and the resulting strains are reported in the Figure 37.

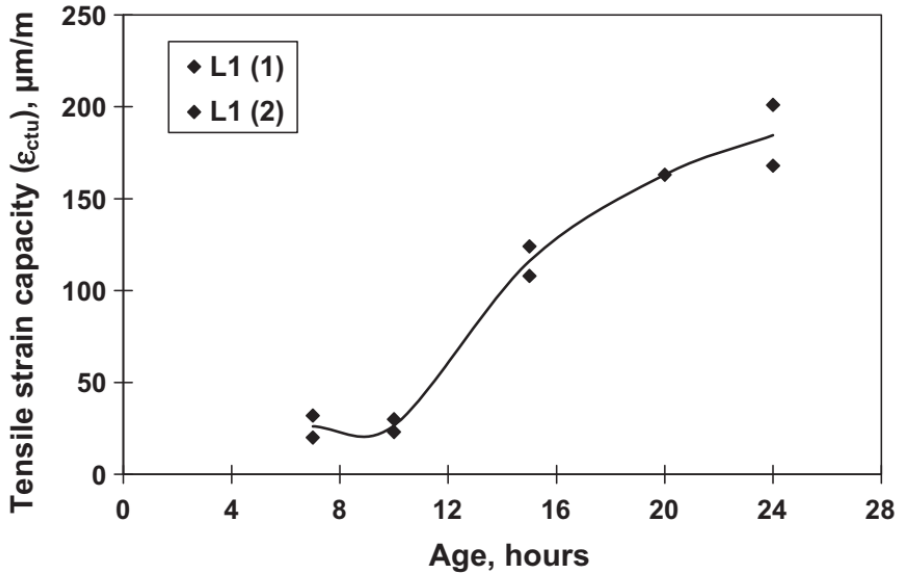

Figure 37: Tensile strain capacity from two sets of tests

Based on these experimental data and the strain capacity prediction model by Eurocode 2 the concrete strain capacity curve is plotted up till 28 days. The strain prediction model defined in section 5.2.4 is used using 28day tensile stress and strain of our original UHPFRCC specimen as a reference. As the exact experimental maximum strains at each day of the concrete are not available at the moment and there is no available information on UHPFRCC maximum strain capacity with time, the available data in hand is used to have a general idea of the trend to maximum strain to compare and understand the behavior with the maximum drying shrinkage strain from our predicted model. The maximum strain capacity curve is shown in Figure 38 where the high strains in the beginning are due to the plastic nature of concrete.

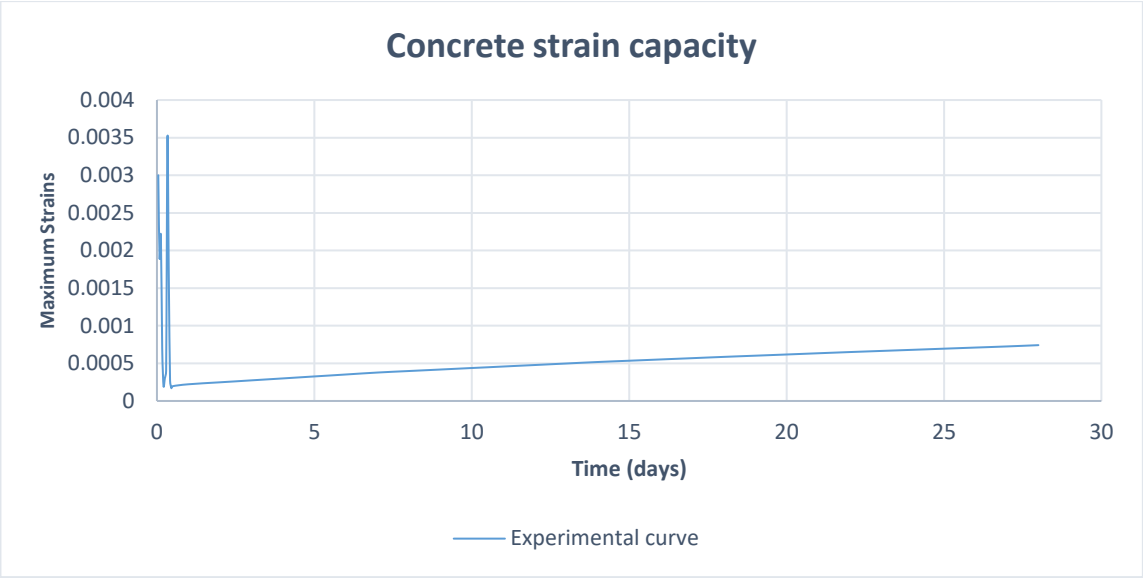

Figure 38: Maximum strain capacity curve

As we have both the strains so we can compare them to find the maximum thickness of our slab. The idea is if the maximum dry shrinkage strains intersect the maximum strain capacity of the concrete then we need to change the concrete slab thickness, increasing the thickness of concrete slab. As increasing the slab thickness will result in lower maximum dry shrinkage strains so at that thickness the slab will have no cracks.

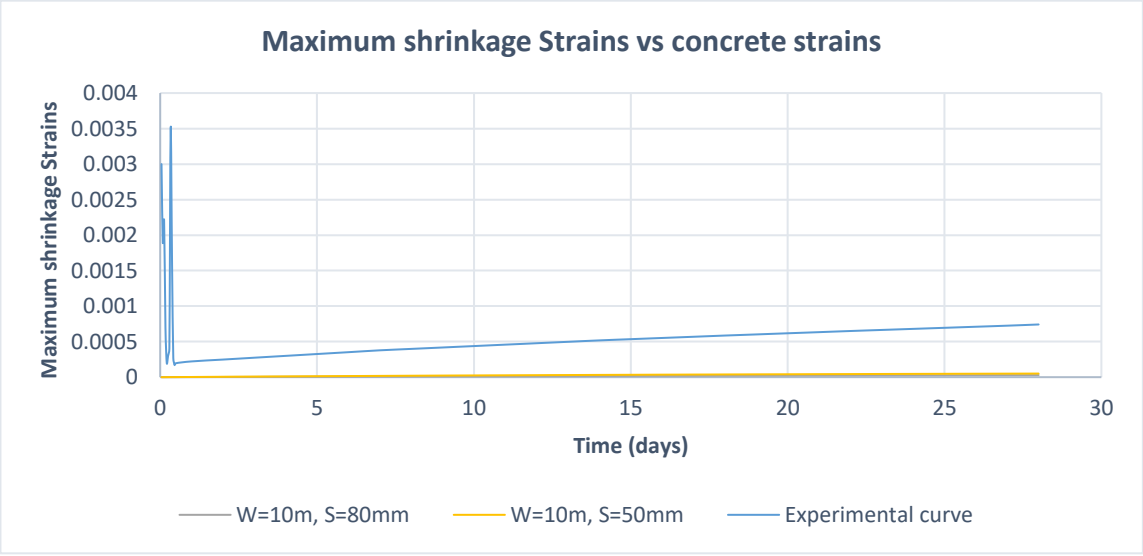

Figure 39: Strain comparison

Figure 39 shows the comparison of maximum shrinkage strains and concrete strain capacity. The dry shrinkage strains are too low as compared to the predicted concrete strain capacity and as a result there is no crack in a slab of 50mm thickness which means in this particular case we can still reduce the thickness until it intersects the allowed strain.

To have the exact comparison of the strains and selecting the required thickness for a crack free slab the only possible solution is to perform the tests on our HPFRCC specimen at different ages.

Different slab widths were also analyzed but changing the slab thickness does not affect the shrinkage results. It is not surprising because in the aspect ratio the exposed width cancels with the width in area and thickness is the only governing parameter.

6. Possible test

To validate the proposed model for prediction of strains in the concrete, some tests can be performed in order to check whether the suggested model is working accurately or not. Test model includes a steel plate on which our HPFRCC slab will lie and a number of strain gauges for measuring strains.

6.1 Material properties

Materials to be used for the test are Steel plate and UHPFRCC slab and their properties are described below.

Tensile Strength

Tensile strength of a material is its capacity, without failure or plastic deformation, to withstand an applied load. Material strength essentially takes into account relationship between the applied external loads on a material and its resulting change in the dimensions or deformations. Tensile strength is the maximum amount of load a material can bear before its failure and ultimate tensile stress is the maximum value of tensile stress on the stress strain curve. Ultimate strength is the maximum stress value on a stress strain curve and then the stress starts to decrease while strain or deformations can increase.

Yield strength

On a stress strain curve, the shift from the elastic behavior to the plastic behavior is represented by yield point. Stress at which plastic deformation of a material starts is known as yield stress while where elastic plus plastic, nonlinear deformation starts is the yield point. Before the yield point, the material has the ability to return to its original shape after the removal of load, but the deformations are permanent after yield point and material can no longer return to its original shape.

Modulus of elasticity

Elastic modulus or modulus of elasticity is assessed by tensile tests and represents uniaxial deformation in linear elastic regime for tensile and compressive stresses. Upon the removal of the load the body can recover its shape up to a limiting value of stress.

6.1.1 Steel properties

Table 7: Steel plate properties

	Min	Max
Ultimate Tensile strength (Mpa)	310	360
Yeild Strength (Mpa)	180	240
Modulus of Elasticity (Gpa)	200	210

6.1.2 UHPFRCC properties

For mechanical properties of slab, the most important are tensile stress and strain properties and elastic modulus. As UHPFRCC is described earlier in detail, below are the properties to be used for performing test.

Table 8: Concrete specimen properties

mechanical properties of concrete		
shrink strain (negative)	erit=	-1.64E-04
Elastic modulus (Mpa)	Ec=	30000
cracking strength (Mpa)	fct=	3
ultimate strength (Mpa)	fu=	4
maximum tens. strain	eu=	0.002
compressive strength (Mpa)	fc=	30
maximum comp. strain	euc=	-0.001

6.2 Geometrical properties of specimens

Geometry of steel plate can be fixed while for UHPFRCC slab two specimens can be considered with the fixed width for both specimen but different thicknesses. An initial thickness can be proposed based on the numerical analysis performed earlier.

Geometrical properties of steel plate and HPFRCC slab can be defined as in table below.

Table 9: Geometrical properties of specimen

	Thickness (t)	Width (w)
Steel plate	3 cm	50 cm
Concrete slab 1	5 cm	40 cm
Concrete slab 2	3 cm	40 cm

The dimensions of steel plate and slab need to be defined to avoid cracks for the first time to simulate results with the proposed model whose results are mentioned already and then changing the slab dimensions to have the cracks in a reduced thickness.

- Choosing thickness t_1 = 5 cm and width w = 40 cm of HPFRCC to avoid crack.
- Choose thickness t_2 = 3 cm and width w = 40 cm of HPFRCC to have a crack.

6.3 Instrument

Instrument used for measuring the strain in order to compare with the strains from the model is strain gauge. Strain gauges measure the effect of external forces as well as external strains on an object. Strain measured directly by strain gauge can lead to the indirect measurements of deflection, pressure, torque, and many other measurements. Intimate contact between the strain gauge and the substrate is crucial for reliable measurement of strain. Based on mounting the strain gauge are classified into two categories, bonded/glued and non-bonded.

A strain gauge usually consists of a fine foil which is bonded in the direction of the applied force to a surface. In order to minimize the negative effect of the Poisson's Strain, the cross-sectional area of the system is decreased. Strain gauges are commonly categorized into bonded resistance and bonded metallic strain gauges. A thin backing material which is attached directly to the test body is bonded with the foil grid. Foil grid directly receives the stress endured by the object, which then responds to a linear change in electrical resistance (mostly linear change).

Hence, proper mounting of strain gauge is crucial to its performance, it ensures that strain applied to the material is correctly transferred to the foil itself via the adhesive and backing material. Strain gauge needs to be glued/bonded on the interface between steel plate and HPFRCC slab in our case. Number of strain gauges to be used in the test are nine in total with three sets in each row as illustrated in Figure 40,Figure 42. First set of gauges at the center of slab and the other two at corners.

6.4 Simulation of test with the model

Based on the results found from the numerical analysis of our proposed model and comparing with data that could be obtained from past researches, the thickness of slab to avoid cracking is 5 cm. This thickness is considered for the initial test to check if the predicted strain from the model is practical or not. The idea is to measure maximum shrinkage strains from the time after concrete pouring when dry shrinkage starts until the concrete achieves full strength at 28^{th} day.

As two series of tests need to be performed to have or to avoid the crack, the first specimen of 5cm HPFRCC slab will be cast and, with the help of strain gauges, the strains will be measured from the start of drying period until 28^{th} day. Strain in the concrete slab will be measured by the strain gauges installed and hence we have the practical results of the maximum value of the state of strain in our concrete specimen. If the model works accurately, then there should be no cracks in the slab because in numerical analysis the maximum strains predicted from the model does not intersect the strains obtained from

experimental data from past researches. These experimental results can be compared with the numerical results to check the reliability of the model.

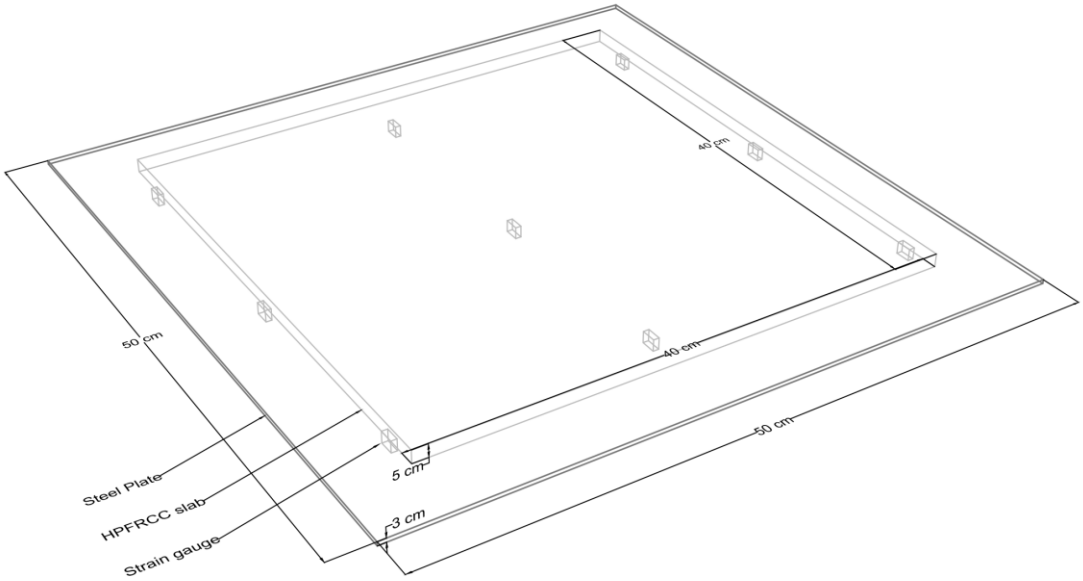

Figure 40: Proposed test model slab 5cm and steel plate 3cm

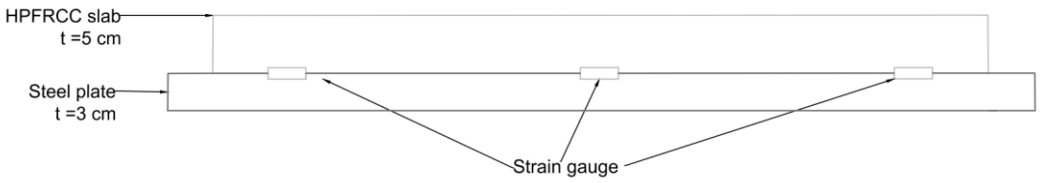

Figure 41: Proposed test model sectional view

For the second specimen, the slab of 3cm in thickness will be cast and maximum strains in the slab will be measured from the start of drying period until 28th day (when concrete reaches full strength). In this thickness there is a possibility of having cracks in the slab, which means the thickness is not sufficient to avoid cracking and needs a new thickness (i.e., increased thickness t).

Changing thickness means increasing thickness in our case because increasing specimen size results in decrease in drying shrinkage and decrease in the maximum state of stress and strain in concrete, hence avoiding cracking.

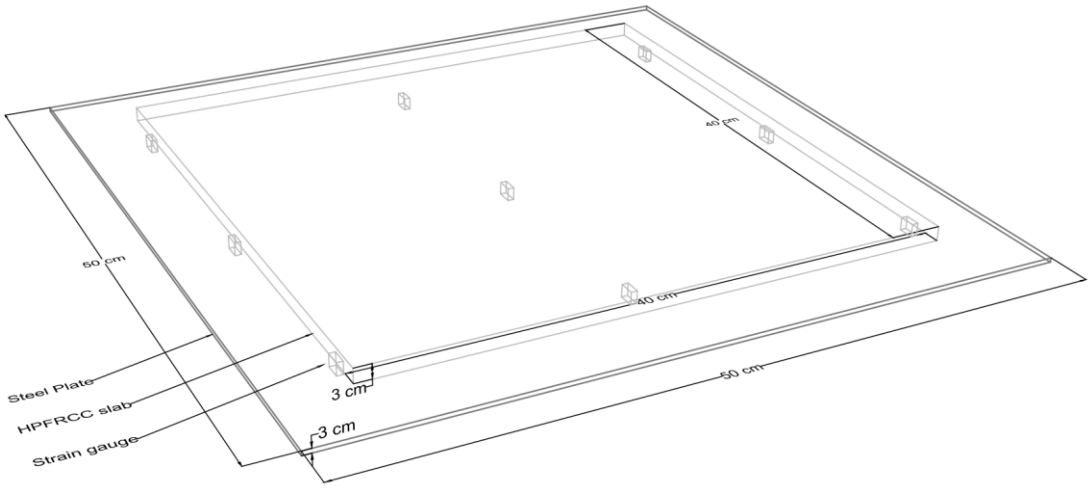

Figure 42: Proposed test model slab 3cm and steel plate 3cm

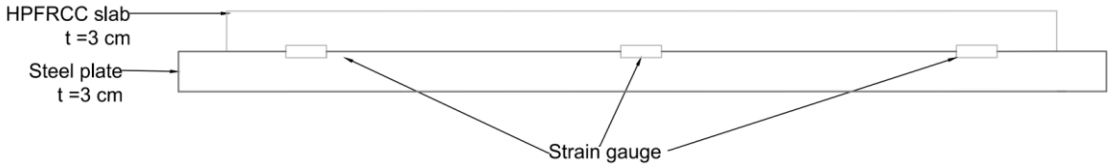

Figure 43: Proposed test model sectional view

It is possible that we do not have cracks in neither t_1 nor in t_2 or we can have cracks in both thicknesses as the parameters defined are general parameters and not the real ones, but this is the only way to verify the model without knowing the material properties at early-age.

7. Conclusion

Tensile strain capacity of concrete is important for controlling cracks in concrete slab and to build crack free slabs on ground. Current methods of finding tensile properties in FRC can not be applied on HPFRCC since strain localization in tension does not occur at cracking, so better prediction models are required in case of HPFRCC.

A possible model for predicting state of stresses and strains is proposed in this thesis which is based on Colonnetti's theory of elastic coaction to define the HPFRCC slab thickness on ground. If the maximum strain in the concrete is lower than the strain capacity, then there will be no crack in the slab. Maximum tensile strain development in concrete with respect to time showed that increase in the slab thickness results in decrease of dry shrinkage strains and in return decreasing the maximum tensile strains developed in the concrete due to shrinkage. A possible test model is also described to verify the proposed theoretical model to be used in future to verify the validity of the proposed approach.

Bibliography

[1] F. H. dministration. [Online]. Available: www.fhwa.dot.gov.

[2] M.-J. K. e. a. Doo-Yeol Yoo, "Effects of mix proportion and curing condition on shrinkage behavior of HPFRCCs with silica fume and blast furnace slag," *Construction and Building Materials 166 (2018) 241–256,* pp. 241-256, 2018.

[3] J. S. P. W. T. J. S. Y. CHOI, "A Study on the Shrinkage Control of Fiber Reinforced Concrete Pavement," *Procedia Engineering,* vol. 14, p. 2815–2822, 2011.

[4] P. Jeong-Hoon Choi and Roger H. L. Chen, "Design of Continuously Reinforced Concrete Pavements Using Glass Fiber," 2005.

[5] J.-J. P. a. S.-W. K. Doo-Yeol Yoo, "Fiber pullout behavior of HPFRCC: Effects of matrix strength and fiber type," *Composite structure,* vol. 174, pp. 263-276, 2017.

[6] K. S. L. J. Y. Y. Yoo DY, "Effect of shrinkage reducing admixture on tensile and flexural behaviors of UHPFRC considering fiber distribution," *Cem Concr Res,* vol. 54, pp. 180-190, 2013.

[7] A. E. N. a. G. J. P.-M. Shih-Ho Chao, "Bond Behavior of Reinforcing Bars in Tensile Strain-Hardening Fiber-Reinforced Cement Composites," *ACI Structural Journal,* 2009.

[8] E. B. Burger A.F, "Experience with the construction of an ultrathin continuously reinforced concrete pavement," *11th International Symposium on concrete roads,* 2010.

[9] N. J. K. S. Hachiya Y., "Applicability of concrete with high flexural strength to airport pavements," *10th International Symposium on Concrete Roads,* 2006.

[10] A.-T. R., "Renewal of concrete slabs using high performance concrete," *9th International Symposium on concrete roads,* 2004.

[11] B. F. Graybeal B, "Development of a Direct Tension Test Method for UHPFRC," *ACI Mater J, ,* vol. 110, pp. 177-186, 2013.

[12] K. H. K. Mahdi Valipour, "Coupled effect of shrinkage-mitigating admixtures and saturated lightweight sand on shrinkage of UHPC for overlay applications," *Construction and Building Materials,* vol. 184, pp. 320-329, 2018.

[13] K. N. P. Ramadoss, "Tensile strength and durability characteristics of high-performance fiber reinforced concrete," *Arabian J Sci Eng,* vol. 33 (2B), pp. 307-319, 2008.

[14] L. M. M. V.Savino, "Simple and effective models to predict the compressive and tensile strength of HPFRC as the steel fiber content and type changes," *Composites Part B: Engineering,* vol. 137, pp. 153-162, 2018.

[15] L. L. A. T. M. V. V. Savinoa, "An extended model to predict the compressive, tensile and flexural strengths of HPFRCs and UHPFRCs: Definition and experimental validation," *Composites Part B ,* vol. 163, pp. 681-689, 2019.

[16] Y. Y. B. M. Xavier Destrée, "Sequential Cracking and Their Openings in Steel-Fiber-Reinforced Joint-Free Concrete Slabs," *J. Mater. Civ. Eng.,* pp. 2-4, 2016.

[17] M. C. P. Richard, "Composition of reactive powder concretes," *Cem. Concr. Res.,* vol. 25, pp. 1501-511, 1995.

[18] H. M. a. P. V. A. P. Fantilli, "Strain Compatibility between HPFRCC and Steel Reinforcement," *Materials and Structures,* vol. 38, 2005.

[19] M. P. a. M. PJM, "Concrete: Microstructure, Properties, and Materials," *Concrete:Microstructure, Properties, and Materials,* vol. 3rd edn., no. McGraw-Hill, New York, USA, 2006.

[20] Bentur, "Early-age Cracking in CementitiousSystems. RILEM Technical Committee 181-EAS: Early-ageShrinkage Induced Stresses and Cracking in CementitiousSystems," RILEM, 2003.

[21] H. e. al., "Cracking tendency of HSC :Tensile strength and self generated stressin the period of setting and early hardening," *Materials and Structures Journal 40(3),* pp. 319-324, 2007.

[22] N. a. Soliman, "Early-age properties of concrete:overview of fundamental conceptsand state-of-the-art research," *Construction Materials,* pp. 12-13, 2009.

[23] V. K. G. B. D. S. W. S. A. Gribniak, "“Investigation of shrinkage of concrete mixtures used for bridge construction in Lithuania," *The Baltic Journal of Road and Bridge Engineering,* vol. 6, pp. 77-83, 2011.

[24] C. T. M. L. M.H. Zhang, "Effect of water-to-cementitious materials ratio and silica fume on the autogenous shrinkage of concrete.," *Cem. Concr. Res.,* vol. 10, p. 687–1694., 2003.

[25] M.-J. K. S. K. G.-S. R. K.-T. K. Doo-Yeol Yoo, "Effects of mix proportion and curing condition on shrinkage behavior of HPFRCCs with silica fume and blast furnace slag," *Construction and Building Materials,* vol. 166, p. 241–256, 2018.

[26] M. L. N. Gardner, " Design provisions for drying shrinkage and creep of normal strength concrete," *ACI Mater. J.,* vol. 98, pp. 159-167, 2001.

[27] S. B. Z. Bazant, "Creep and Shrinkage Prediction Model for Analysis and Design of Concrete Structures: Model B3," *ACI Special Publications,* vol. 194, pp. 1-84, 2000.

[28] Y. O. a. S. Kan, "Effects of specimen size on strength and drying shrinkage of polymer-modified concrete," *The International Journal of Cement Composites and Dghtweight Concrete,* vol. 4, pp. 229-233, 1982.

[29] P. H. Lenka Dohnalová, "SIZE EFFECT ON THE ULTIMATE DRYING SHRINKAGE OF CONCRETE - EXPERIMENTAL EVIDENCE AND ENGINEERING PRACTICE," *Acta Polytechnica CTU Proceedings,* vol. 26, pp. 13-18, 2020.

[30] W. P. B. Riaan Combrinck, "Tensile properties of plastic concrete and the influence of temperature and cyclic loading," *Cement and Concrete Composites,* vol. 97, pp. 300-311, 2019.

[31] T. A. Hammer, "Deformations, strain capacity and cracking of concrete in plastic and early hardening phases," Fakultet for ingeniørvitenskap og teknologi, 2007.

[32] R. C. A. L. Emmanuel Roziere, "Tensile behaviour of early age concrete: New methods of investigation," *Cement & Concrete Composites ,* vol. 55, pp. 153-161, 2015.

[33] 1. (AASHTO, "AASHTO GUIDE FOR DESIGN OF PAVEMENT STRUCTURES". America 1993.

[34] N. a. F. Tehmina, "Mechanical Properties of High-Performance Concrete Reinforced with Basalt Fibers," *Procedia Engineering 77,* pp. 31-139, 2014.

[35] K. S. R. M. A. Sumathi, "Study on the strength and durability characteristics of high strength concrete with steel fibers," *Int J ChemTech Res,* vol. 8 (1), pp. 241-248, 2015.

[36] *Deformations, strain capacity and cracking of concrete in plastic and early hardening phases,* 2007.

8. Annex

8.1 Excel macro of model

```
Public Ec As Double 'modulo elastico del cls
Public Et As Double 'modulo elastico del terreno in superficie
Public fct As Double 'resistenza alla fessurazione
Public fu As Double 'resistenza ultima a trazione
Public eu As Double 'deformazione ultima a trazione
Public fc As Double 'resistenza a compressione

Option Explicit
Dim PageBreakState As Variant

Sub startProcess()
   OptimizationStart
   init
   OptimizationEnd
End Sub

Function OptimizationStart(Optional ByVal ibBlinkStatusBar As Boolean = True, Optional ByVal
ibSetCursorHourglass As Boolean = False)
   Application.ScreenUpdating = False
   Application.EnableEvents = False
   'disable formulas calculations
   Application.Calculation = xlCalculationManual
   'disable page break calculation
   PageBreakState = ActiveSheet.DisplayPageBreaks
   ActiveSheet.DisplayPageBreaks = False
   Application.DisplayStatusBar = False
```

```
    Application.Cursor = xlWait
End Function

Function OptimizationEnd()

    Application.DisplayStatusBar = True
    ActiveSheet.DisplayPageBreaks = PageBreakState
    Application.Calculation = xlCalculationAutomatic
    Application.EnableEvents = True
    Application.ScreenUpdating = True
    Application.Cursor = xlDefault
End Function


Function init()
    Dim startVal, endVal, inc, currentVal  As Double
    Dim repetitionCount, maxRepetitions As Integer
    Dim found As Boolean

    found = False

    maxRepetitions = Range("C14").Value
    repetitionCount = 0
    inc = Range("C15").Value
    currentVal = Range("D5").Value
    found = True

    Do Until executeProcess = True
        found = False
        Range("D5").Value = currentVal
```

```
        currentVal = currentVal + inc

        If repetitionCount = maxRepetitions Then
            Exit Do
        End If
        repetitionCount = repetitionCount + 1

        found = True
    Loop

    If found = True Then
        MsgBox "Soil thickness found having at max one positive value, Soil Thickness: " &
currentVal & _
            vbLf & "Number of iterations done: " & repetitionCount + 1

    Else
        MsgBox "Soil thickness not found. Max repetitions reached " & maxRepetitions
    End If
End Function



Function executeProcess() As Boolean

' Main per il calcolo degli effetti del ritiro
'
Dim A0 As Double 'area omohñgenizzata
Dim B As Double 'base della sezione
Dim enl1(100) As Double 'deformazione impressa di nonlinearitö nello strato 1
Dim enl2(100) As Double 'deformazione impressa di nonlinearitö nello strato 2
Dim erit As Double 'deformazione di ritiro
Dim def As Double 'valore della deformazione di una striscia
```

```
Dim delam As Double 'incremento di deformazione impressa

Dim demu As Double 'incremento di curvatura impressa

Dim deltadefimp1(100) As Double 'incremento di deformazione impressa in una striscia del 1Á strato

Dim deltadefimp2(100) As Double 'incremento di deformazione impressa in una striscia del 2Á strato

Dim i As Integer 'variabile dei cicli

Dim Jx0 As Double 'momento d'inerzia della sezione

Dim lambda As Double ' parametro di deformazione

Dim Mris As Double 'risultamnte del momento flettente

Dim mu As Double 'curvatura della sezione

Dim n As Double 'coefficiente di omogenizzazione

Dim nordep As Double ' norma dell'incrmento di deformazione impressa

Dim Nris As Double 'risultamnte dello sforzo normale

Dim s As Double 'altezza della parte di cls

Dim S0 As Double 'momento statico della sezione rispetto al bordo inferiore

Dim S0c As Double 'momento statico della parre di calcestruzzo rispetto al baricentro dell'inytera sezione

Dim st As Double 'altezza della parte di terreno

Dim tens1(100) As Double 'valore di tensione di regime linere in una striscia nello strato 1

Dim tens2(100) As Double 'valore di tensione di regime lineare in una striscia nello strato 2

Dim tensnl1(100) As Double 'valore di tensione di regime nonlineare in una striscia nello strato 1

Dim tensnl2(100) As Double 'valore di tensione di regime nonlineare in una striscia nello strato 2

Dim y1(100) As Double 'posizione della striscia rispetto al baricentro nello strato 1

Dim y2(100) As Double 'posizione della striscia rispetto al baricentro nello strato 2

Dim yg As Double 'posizione del baricentro rispetto al bordo inferiore


Dim isPositive As Boolean

   'memorizzo le variabili
```

```
Range("D3").Select
B = ActiveCell.Value

Range("D4").Select
s = ActiveCell.Value

Range("D5").Select
st = ActiveCell.Value

Range("H3").Select
erit = ActiveCell.Value

Range("H4").Select
Ec = ActiveCell.Value

Range("H5").Select
fct = ActiveCell.Value

Range("H6").Select
fu = ActiveCell.Value

Range("H7").Select
eu = ActiveCell.Value

Range("H8").Select
fc = ActiveCell.Value


Range("L6").Select
Et = ActiveCell.Value
```

```
'proprietš geometriche in regime lineare elastico

n = Et / Ec 'coefficiente di omogenizzazione
A0 = B * s + n * B * st 'area omogenizzata della sezione
S0 = B * s * (st + s / 2) + n * B * st ^ 2 / 2 'momento statico
yg = S0 / A0 'baricentro rispetto al bordo inferiore
Jx0 = B * s ^ 3 / 12 + B * s * (s / 2 + st - yg) ^ 2 + n * (B * st ^ 3 / 12 + B * st * (yg - st / 2) ^ 2)
'momento d'inerza della sezione

'valori iniziali dei parametri di deformazione
lambda = B * erit / A0 * s

S0c = B * s * (yg - s / 2 - st) 'momento statico dell'area di calcestruzzo

mu = erit / Jx0 * S0c 'curvatura della sezione



'stato tensionale nella sezione nell'ipotesi di comportamento lineare
Range("N2").Select
Nris = 0
Mris = 0

'primo strato
For i = 0 To 100
  y1(i) = yg - st / 100 * i
  def = lambda + mu * y1(i)
```

```
    ActiveCell.Value = y1(i)
    ActiveCell.Offset(0, 1).Select
    tens1(i) = Et * def
    ActiveCell.Value = tens1(i)
    ActiveCell.Offset(1, -1).Select
  Next i

  'secondo strato
  For i = 0 To 100
    y2(i) = yg - st - s / 100 * i
    def = lambda + mu * y2(i)
    ActiveCell.Value = y2(i)
    ActiveCell.Offset(0, 1).Select
    tens2(i) = Ec * (def - erit)
    ActiveCell.Value = tens2(i)
    ActiveCell.Offset(1, -1).Select

  Next i

  'calcolo delle risultati
  Nris = 0
  Mris = 0
  'primo strato
  For i = 1 To 99 Step 2
    Nris = Nris + B * (4 * tens1(i) + tens1(i - 1) + tens1(i + 1)) / 6 * Abs(y1(i + 1) - y1(i - 1))

    Mris = Mris + B * (4 * tens1(i) * y1(i) + tens1(i - 1) * y1(i - 1) + tens1(i + 1) * y1(i + 1)) / 6 *
Abs(y1(i + 1) - y1(i - 1))

  Next i
  'secondo strato
```

```
For i = 1 To 99 Step 2
   Nris = Nris + B * (4 * tens2(i) + tens2(i - 1) + tens2(i + 1)) / 6 * Abs(y2(i - 1) - y2(i + 1))

   Mris = Mris + B * (4 * tens2(i) * y2(i) + tens2(i - 1) * y2(i - 1) + tens2(i + 1) * y2(i + 1)) / 6 *
Abs(y2(i + 1) - y2(i - 1))

Next i


Range("P2").Select
ActiveCell.Value = Nris

Range("q2").Select
ActiveCell.Value = Mris

Range("P4").Select
ActiveCell.Value = lambda

Range("q4").Select
ActiveCell.Value = mu

'parte nonlineare


Do
nordep = 0
'calcolo delle deformazioni impresse di risposta nonlineare
   'primo strato
   For i = 0 To 100
      def = lambda + mu * y1(i) - enl1(i)
      deltadefimp1(i) = (Et * def - sigt(def)) / Et
```

```
        nordep = nordep + Abs(deltadefimp1(i))
        enl1(i) = enl1(i) + deltadefimp1(i)
    Next i
    'secondo strato
    For i = 0 To 100
        def = lambda + mu * y2(i) - erit - enl2(i)
        deltadefimp2(i) = (Ec * def - sigc(def)) / Ec
        nordep = nordep + Abs(deltadefimp2(i))
        enl2(i) = enl2(i) + deltadefimp2(i)
    Next i

  'calcolo di deltaLambda e deltamu dovute alla nonlinearitö
    delam = 0
    demu = 0
    'primo strato
    For i = 1 To 99 Step 2
        delam = delam + B / A0 / Ec * (Et * deltadefimp1(i + 1) + Et * deltadefimp1(i - 1) + 4 * Et *
deltadefimp1(i)) / 6 * Abs(y1(i + 1) - y1(i - 1))
        demu = demu + B / Jx0 / Ec * (Et * deltadefimp1(i + 1) * y1(i + 1) + Et * deltadefimp1(i -
1) * y1(i - 1) + 4 * Et * deltadefimp1(i) * y1(i)) / 6 * Abs(y1(i + 1) - y1(i - 1))


    Next i
    'secondo strato
    For i = 1 To 99 Step 2


        delam = delam + B / A0 / Ec * (Ec * deltadefimp2(i + 1) + Ec * deltadefimp2(i - 1) + 4 * Ec
* deltadefimp2(i)) / 6 * Abs(y2(i + 1) - y2(i - 1))


        demu = demu + B / Jx0 / Ec * (Ec * deltadefimp2(i + 1) * y2(i + 1) + Ec * deltadefimp2(i -
1) * y2(i - 1) + 4 * Ec * deltadefimp2(i) * y2(i)) / 6 * Abs(y2(i + 1) - y2(i - 1))
```

```
    Next i


    Range("P5").Select
    ActiveCell.Value = delam

    Range("q5").Select
    ActiveCell.Value = demu




    'aggiornamento dei parametri di deformazione
    lambda = lambda + delam
    mu = mu + demu

    If nordep < Abs(B * erit / A0 * s) / 10000000000# Then
       Exit Do
    End If



Loop


'stato tensionale nella sezione nell'ipotesi di comportamento nonlineare
Range("s2").Select
```

```
Nris = 0
Mris = 0

Dim countPositive As Integer

countPositive = 0
'primo strato
For i = 0 To 100
   def = lambda + mu * y1(i) - enl1(i)
   tensnl1(i) = Et * def
   ActiveCell.Value = tensnl1(i)

   If tensnl1(i) > 0 Then

      If countPositive >= 1 Then
         isPositive = True
         executeProcess = Not isPositive

         Exit Function
      Else
         countPositive = countPositive + 1
      End If

   End If

   ActiveCell.Offset(0, 1).Select
   ActiveCell.Value = lambda + mu * y1(i)

   ActiveCell.Offset(1, -1).Select
Next i
```

```
If countPositive <> 1 Then
   isPositive = True
   executeProcess = Not isPositive
   Exit Function
End If

'secondo strato
For i = 0 To 100
   def = lambda + mu * y2(i) - erit - enl2(i)
   tensnl2(i) = Ec * def
   ActiveCell.Value = tensnl2(i)
   ActiveCell.Offset(0, 1).Select
   ActiveCell.Value = lambda + mu * y2(i) - erit
   ActiveCell.Offset(1, -1).Select
Next i


'calcolo delle risultati
Nris = 0
Mris = 0
'primo strato
For i = 1 To 99 Step 2
   Nris = Nris + B * (4 * tensnl1(i) + tensnl1(i - 1) + tensnl1(i + 1)) / 6 * Abs(y1(i + 1) - y1(i - 1))

   Mris = Mris + B * (4 * tensnl1(i) * y1(i) + tensnl1(i - 1) * y1(i - 1) + tensnl1(i + 1) * y1(i + 1)) /
6 * Abs(y1(i + 1) - y1(i - 1))

Next i
'secondo strato
For i = 1 To 99 Step 2
```

```
        Nris = Nris + B * (4 * tensnl2(i) + tensnl2(i - 1) + tensnl2(i + 1)) / 6 * Abs(y2(i + 1) - y2(i - 1))

        Mris = Mris + B * (4 * tensnl2(i) * y2(i) + tensnl2(i - 1) * y2(i - 1) + tensnl2(i + 1) * y2(i + 1)) /
6 * Abs(y2(i + 1) - y2(i - 1))

    Next i



    Range("P8").Select
    ActiveCell.Value = Nris

    Range("q8").Select
    ActiveCell.Value = Mris

    Range("P9").Select
    ActiveCell.Value = lambda

    Range("q9").Select
    ActiveCell.Value = mu




    executeProcess = Not isPositive


'!!!!!!!!!!!!!!!!!!!!!!!!!!!!!!!!!!
'prova leggi
'Sheets("Foglio1").Select
'Range("N1").Select
'For i = 0 To 30
```

```
'    def = -0.01 + 0.001 * i
'    ActiveCell.Value = def
'    ActiveCell.Offset(0, 1).Select
'    ActiveCell.Value = sigc(def)
'    ActiveCell.Offset(1, -1).Select
'Next i
'Range("N1").Select
'Stop
'!!!!!!!!!!!!!!!!!!!!!!!!!!!!!!!!!!!!


End Function
```